DRL-58-DRD-SE 7

DOE/JPL 954373 - 78/7
Distribution Category UC-63

HEAT EXCHANGER METHOD — INGOT CASTING
FIXED ABRASIVE METHOD — MULTI-WIRE SLICING
PHASE II

Silicon Sheet Growth Development for the
Large Area Sheet Task
of the Low Cost Solar Array Project

QUARTERLY PROGRESS REPORT NO. 4
BY

FREDERICK SCHMID AND CHANDRA P. KHATTAK

Covering Period from July 1, 1978 through September 30, 1978
Date of Report: October 15, 1978

JPL Contract No. 954373

(NASA-CR-158038) SILICON SHEET GROWTH DEVELOPMENT FOR THE LARGE AREA SHEET TASK OF THE LOW COST SOLAR ARRAY PROJECT. HEAT EXCHANGER METHOD - INGOT CASTING FIXED ABRASIVE METHOD - (Crystal Systems, Inc., G3/44 N79-14540 Unclas 41941

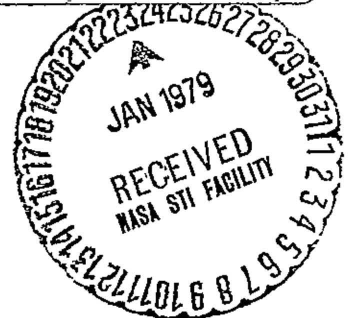

CRYSTAL SYSTEMS INC.

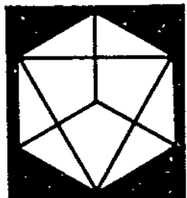

Shetland Industrial Park
35 Congress Street, Salem, Mass. 01970

The JPL Low-Cost Solar Array Project is sponsored by the U. S. Department of Energy and forms part of the Solar Photovoltaic Conversion Program to initiate a major effort toward the development of low-cost solar arrays. This work was performed for the Jet Propulsion Laboratory, California Institute of Technology by agreement between NASA and DOE.

This report contains information prepared by Crystal Systems, Inc., under JPL subcontract. Its content is not necessarily endorsed by the Jet Propulsion Laboratory, California Institute of Technology, National Aeronautics and Space Administration or the U. S. Department of Energy.

TABLE OF CONTENTS

ABSTRACT iii

CRYSTAL CASTING 1

Casting of Square Ingots 1

Improvement of Heat Extraction 5

Solar Cell Performance 7

Process Development 19

CRYSTAL SLICING 30

Blade Development 30

Efforts to Reduce Kerf. 44

Machine Development 50

Process Development 51

CONCLUSIONS 58

REFERENCES 60

MILESTONES 62

ABSTRACT

Solar cells fabricated from HEM cast silicon have yielded up to 15% conversion efficiencies. This has been achieved in spite of using unpurified graphite parts in the HEM furnace and without optimization of material or cell processing parameters.

Molybdenum retainers have prevented SiC formation and reduced carbon content by 50%. The oxygen content of vacuum cast HEM silicon is lower than typical Czochralski grown silicon.

Impregnation of 45 μm diamonds into 7.5 μm copper sheath has shown distortion of the copper layer. However, 12.5 μm and 15 μm copper sheath can be impregnated with 45 μm diamonds to a high concentration. Electroless nickel plating of wires impregnated only in the cutting edge has shown nickel concentration around the diamonds. This has the possibility of reducing kerf.

The high speed slicer fabricated can achieve higher speed and longer stroke with vibration isolation. This machine will be used for slicing 3" and 4" diameter workpieces.

CRYSTAL CASTING

The emphasis in the area of crystal casting during this quarter was to optimize heat flow conditions and develop an understanding of the shape of the solid-liquid interface during growth in circular ingots as well as square shaped ingots. Ingots cast by HEM were characterized and evaluated for solar cell performance.

Casting of Square Ingots

It has been reported earlier[1] that in order to achieve semiconductor purity a high purity liner was used inside a low purity crucible. Such a duplex crucible fabricated by a modified technique was used in run 2-054-C (details in Table I) to cast a square ingot. It was found that the liner was attached to the silicon ingot and severe cracking of silicon resulted. So far the use of a duplex crucible to prevent cracking of the ingot has achieved only limited results.

High purity square crucibles similar to the ones used to cast 6" diameter ingots were received in-house. For ease of fabrication the wall thickness has been increased and sides were slightly tapered. The bottom of the crucible is rather thick; hence, heat extraction without a graphite plug is

TABLE I. TABULATION OF HEAT-EXCHANGER AND FURNACE TEMPERATURES

RUN	PURPOSE	SEEDING		GROWTH CYCLE			REMARKS
				RATE OF DECREASE			
		FURN. TEMP. ABOVE M.P.	H.E. TEMP. BELOW M.P.	H.E. TEMP. °C/HR.	FURN. TEMP. °C	GROWTH TIME IN HOURS	
2-052-C	Test high purity crucible with graphite plug	9	78	202	9	4.75	Power instability toward end of growth cycle. Heater cracked.
2-053-C	Test high purity crucible with graphite plug	-	-	-	-	-	Run aborted. Seed melted out.
2-054-C	Test duplex square crucible	3	208	244	3	7.25	Attachment of crucible has caused cracking of ingot
2-055-C	Test new type of graphite plug	5	135	-	-	-	Run terminated after 3 hrs. into growth cycle because of reaction
2-056-C	Test graphite plug	-	-	-	-	-	Run aborted due to distortion of crucible
2-057-C	Test high purity square crucible	30	202	446	30	5.50	Seed melted out. Attachment of crucible only in bottom area.
2-058-C	Test high purity square crucible	7	434	388	7	4.50	Attachment of crucible to ingot. Good crystallinity.

TABLE I. (Cont.)

RUN	PURPOSE	SEEDING		GROWTH CYCLE			REMARKS
				RATE OF DECREASE			
		FURN.TEMP. ABOVE M.P.	H.E.TEMP. BELOW M.P.	H.E. TEMP. °C/HR.	FURN. TEMP. °C	GROWTH TIME IN HOURS	
2-059-C	Test high purity square crucible	15	289	233	15	4.75	Good crystallinity; some attachment of crucible.
2-060-C	Test high purity square crucible	22	114	316	22	5.0	Attachment of crucible caused cracking of ingot.
2-061-C	Test high purity square crucible	8	103	-	-	-	Run terminated after 2 hrs. because of turbulence in crucible.
2-062-C	Test high purity square crucible	<3	133	-	-	-	Run terminated after 2 hrs. because of turbulence in crucible.
2-063-C	Test high purity 6" Ø crucible	<3	269	307	1	6.0	Turbulence towards end of growth cycle.
2-064-C	Test high purity 6" Ø crucible	14	142	variable	14	6.0	Turbulence during growth cycle.
2-065-C	Test graphite pieces for plugs	-	-	-	-	-	Some plugs cracked on contact with silicon
2-066-C	Test high purity 6" Ø crucible	<3	157	85	3	6.25	Cracking of ingot around periphery only. Turbulence observed.

TABLE I. (Cont.)

RUN	PURPOSE	SEEDING		GROWTH CYCLE			REMARKS
		FURN.TEMP. ABOVE M.P.	H.E.TEMP. BELOW M.P.	RATE OF DECREASE H.E. TEMP. °C/HR.	RATE OF DECREASE FURN. TEMP. °C	GROWTH TIME IN HOURS	
2-067-C	Investigate cause of turbulence during growth	< 3	105	1065	0	4.2	Helium flow control malfunction
2-068-C	Test new plug in high-purity square crucible	3	178	202	-	3.6	Turbulence observed in liquid during growth.
2-069-C	Avoid turbulence during growth	3	239	175	-	3.6	Turbulence observed in liquid during growth
2-070-C	Avoid turbulence during growth	6	375	171	-	4.5	Turbulence observed in liquid during growth
2-071-C	Avoid turbulence during growth	< 3	301	191	3	5.2	No turbulence observed. Very good crystallinity.
2-072-C	Cast square cross-section ingot	5	259	558	-	1.3	Turbulence observed during growth.
2-073-C	Cast 6"Ø ingot	5	311	228	5	4.5	No turbulence observed. Very good crystallinity.

expected to be a problem. It is necessary to achieve a proper graded structure in these crucibles to prevent cracking. Runs 2-057-S through 2-062-C were carried out in high purity square crucibles that were heat treated to develop the graded structure. Solidification of the ingot could only be completed by lowering the furnace temperature below the melt point of silicon. During this process liquid was entrapped and cracked the ingot. Not much information could be obtained about the graded structure of the crucible. In runs 2-061-C and 2-062-C some turbulence was observed in the melt during the growth cycle. Such a phenomenon was not observed with casting of round ingots. It was felt that a graphite plug had to be used to improve heat extraction.

Improvement of Heat Extraction

It has been demonstrated[2] that temperature gradients in the liquid are very important to the crystal growth of silicon by the HEM. High superheat of the melt and thereby steep gradients in the liquid caused low growth rates and polycrystalline growth. Higher thermal conductivity of liquid silicon as compared to the solid state makes heat extraction from the melt difficult. This is further complicated by the fact that the conductivity of silica crucibles drops significantly as the heat exchanger temperature is decreased.[3] Solution of these problems has been achieved by using very low superheat in the melt and by using a graphite plug through a hole in the bottom of the crucible.

High purity crucibles used to cast 6" diameter ingots have a thin wall and a curvature at the bottom. These parameters contribute a degree of complexity to making a leak-proof seal at the plug/crucible joint since the crucible sags and distorts the hole. In runs 2-053-C and 2-056-C higher furnace temperatures resulted in melting of seed, penetration of liquid silicon into the plug, and thereby breakdown of the plug/crucible joint. Evaluation of various graphites was carried out in runs 2-065-C and 2-066-C to study their reaction with molten silicon. It was found that the ATJ grade gave the best results.

The use of the ATJ graphite plug in runs 2-067-C through 2-070-C improved the heat extraction and thereby growth of the ingot. However, when crystal growth was well into the growth cycle, turbulence in the melt was observed. The nature of the turbulence suggests that when the solid-liquid interface progresses during initial stages, there is no problem. However, when the interface grows out and reaches the sides of the crucible, the bottom corner is at the hottest temperature. Thus the interface touches the side of the crucible and traps liquid silicon in the bottom corner. During later stages of the growth cycle, when trapped liquid undergoes expansion on cooling, it squirts liquid silicon and starts turbulence. It was established that some hot spots had developed in the furnace chamber which could lead to this problem. Once the heat flow characteristics were understood, it was corrected in runs 2-071-C and 2-073-C where no turbulence was observed.

As mentioned above, the need for low liquid gradients and high growth rates necessitates a low superheat in the melt. One of the problems encountered as a result of this is that when solidification has progressed, the cooling effect of the heat exchanger causes the furnace temperature to fall below the melting point and causes freezing from the top surface. In order to avoid this effect, a tapered heating element was designed and fabricated which will give a gradient in the furnace. The use of this heater would keep the temperature of the melt close to solidification temperature in proximity to the interface and avoid the freezing of liquid near the top surface. Such heater was used starting with run 2-071-C and no freezing occurred from the top surface.

Solar Cell Performance

During last quarter[1] it was reported that solar cells with conversion efficiency up to 14% could be fabricated out of HEM cast silicon. These results were obtained in one boule sample (run 2-021-C). Since then a number of boules have been cast in high-purity graded crucibles; hence it was desirable to study the repeatability and performance of devices as a function of variables.

Samples from run 2-048-C, 2-049-C and 2-050-C were fabricated in 2 cm x 2 cm solar cells along with silicon from run 2-021-C (tested earlier also) and evaluated under AMO and AM1 illumination. In order to achieve higher conversion efficiencies <100> seeds were used in these runs so that the cells could be texture etched. However, a solid-liquid interface breakdown occurred in run

2-050-C so the structure of this ingot had large grains and was not single crystal. Some of the samples were fabricated with back surface field and/or texturized. The junctions of all the cells were diffused in the same batch. The solar cell characteristics of the control cells are tabulated in Table II, those of polished test samples in Table III, and BSF and/or texturized cells in Table IV. The AM1 efficiencies are derived from test measurements. The nominal cell thicknesses are 9±1 mils, test temperature is 25±2°C and illumination is 135.3 mW/cm^2 (AM1), 100 mW/cm^2 (AMO).

The control samples were made from 1-3 Ω-cm CZ silicon. The "F," "C" and "B" cells in Table II refer to front, center and back positions respectively in the diffusion tube. A review of the data shows that there is no evidence of cross-contamination between ingots. This is expected as all the ingots were cast under similar conditions in the HEM furnace.

A review of data in Table III for polished wafers shows that cells from 2-021-C ingot show conversion efficiency of up to 14.1%. This is comparable to the value of 14% reported earlier.[1] Good performance was achieved for the other ingots, i.e., conversion efficiencies higher than 13% are obtained. It should be noted that ingot 2-050-C where single crystallinity was not achieved, a conversion efficiency of 13% has been obtained.

In Table IV the solar cell data is reported for cells with BSF and/or texturization. Samples from 2-021-C were not sculptured as they had <111> orientation. A comparison of data in Table III

and Table IV shows that not much improvement in cell performance is observed for 2-021-C samples with BSF. However, 2-048-C and 2-049-C do show improvement in I_{sc} values, slight increase in V_{oc} value and degradation of CFF values, resulting in overall enhancement of conversion efficiency with BSF and texturization. Samples from 2-050-C show an overall degradation with only slight improvement in I_{sc} values. This can be explained because this ingot was not single crystal and BSF and texturization may have resulted in shunting across the grain boundaries. In Table V the results of best cells of each lot are tabulated and it can be seen that the maximum enhancement of conversion efficiency with BSF has been achieved for samples with the highest resistivity (3.2 to 3.7 Ω-cm) which is as expected. It is felt that for an HEM cast silicon with resistivity about 10 Ω-cm further improvement in cell performance can be expected.

The HEM silicon in the test runs has been cast in a contaminated furnace. The graphite parts replaced have not even been purified and are known to have high impurity content, yet the solar cells fabricated are very near the state-of-the-art production values. Possibly the 0.1 torr vacuum minimizes the effect of volatile impurities.

Solar cell Nos. 4 and 6 from run 2-021-C reported in the last quarterly were measured for diffusion length and the values obtained were 106 and 99 μm respectively.

At the present time, spectral response and diffusion length data has not been taken on these cells. During testing the factors

for converting AMO I_{sc}, V_{oc} and η values to AM1 values were measured and are summarized for each lot in Table VI. It can be seen that these factors have similar values indicating that the performance of the HEM silicon is rather consistent. Representative cells from each lot will be measured for their spectral response.

TABLE II. SOLAR CELL CHARACTERISTICS OF CONTROL CELLS

Cell Number	AMO I_{sc} (mA)	AMO V_{oc} (mV)	AMO η	CFF	AM1 η
F-1	137	608	12.2	0.79	14.3
F-2	140	612	12.4	0.78	14.5
F-3	140	613	12.5	0.79	14.6
C-1	144	608	12.8	0.79	15.0
C-2	142	612	12.6	0.78	14.8
C-3	141	611	12.4	0.78	14.5
B-1	143	608	12.4	0.77	14.5
B-2	143	610	12.6	0.78	14.8

TABLE III. SOLAR CELL CHARACTERISTICS OF TEST SAMPLES; THE CELLS ARE MADE ON POLISHED WAFERS

Ingot	#	AMO I_{sc} (mA)	AMO V_{oc} (mV)	AMO η	CFF	AM1 η
2-021-C	1	139	605	10.4	0.67	12.2
	2	136	607	11.2	0.74	13.1
	3	141	616	11.9	0.74	14.0
	4	135	580	7.8	0.54	9.1
	5	138	603	10.5	0.68	12.3
	6	140	583	8.3	0.55	9.7
	7	140	607	10.7	0.68	12.6
	8	139	618	12.0	0.76	14.1
2-048-C	1	134	573	11.0	0.78	12.8
	2	134	574	10.9	0.76	12.7
	3	133	574	11.0	0.78	12.8
	4	133	573	10.8	0.77	12.6
	5	132	572	11.0	0.79	12.8
	6	133	575	11.2	0.79	13.1
	7	131	576	11.0	0.79	12.8
	8	133	575	10.9	0.77	12.7

. . Cont'd.

TABLE III. (Cont'd.)

Ingot	#	AMO I_{sc} (mA)	AMO V_{oc} (mV)	AMO η	CFF	AM1 η
2-049-C	1	128	568	10.4	0.77	12.2
	2	137	573	11.5	0.79	13.5
	3	136	572	11.3	0.79	13.3
	4	134	569	11.0	0.78	13.0
	5	136	573	11.5	0.80	13.5
	6	133	567	10.8	0.77	12.7
	7	133	569	11.0	0.79	13.0
	8	132	568	10.8	0.78	12.7
2-050-C	1	127	594	10.7	0.77	12.5
	2	126	582	8.7	0.64	10.2
	3	129	598	10.9	0.77	12.8
	4	129	592	10.0	0.71	11.7
	5	127	597	10.9	0.78	12.8
	6	128	599	11.1	0.78	13.0
	7	128	594	10.3	0.73	12.1
	8	126	594	10.7	0.78	12.5

TABLE IV. SOLAR CELL CHARACTERISTICS OF TEST SAMPLES.
THE DEVICES HAVE BSF AND/OR TEXTURIZATION

Ingot	Orientation	BSF	Texturized	#	AMO I_{sc} (mA)	AMO V_{oc} (mV)	AMO η	CFF	AM1 η
2-021-C	(111)	Yes	No	1	142	606	11.0	0.69	12.9
				2	135	605	10.4	0.69	12.2
				3	135	603	10.4	0.69	12.2
				4	140	607	10.0	0.64	11.7
				5	142	617	11.8	0.73	13.8
				6	140	617	12.0	0.75	14.1
				7	135	606	11.3	0.75	13.2
				8	133	600	10.3	0.70	12.1
2-048-C	(100)	Yes	Yes	2	147	578	11.4	0.73	13.3
				3	149	591	12.3	0.76	14.4
				4	147	582	12.2	0.77	14.2
				5	150	587	12.1	0.75	14.1
				6	148	585	11.6	0.72	13.5

.Cont'd.

TABLE IV. (Cont'd.)

Ingot	Orientation	BSF	Texturized	#	AMO I_{sc} (mA)	AMO V_{oc} (mV)	AMO η	CFF	AM1 η
2-049-C	(100)	Yes	Yes	2	148	583	12.2	0.77	14.2
				3	156	591	12.8	0.75	15.0
				4	156	587	11.6	0.69	13.5
				5	156	587	12.5	0.74	14.6
				6	157	591	12.4	0.72	14.5
				7	148	577	11.5	0.73	13.4
				8	149	583	12.0	0.75	14.0
2-050-C	Poly	Yes	Yes	1	137	588	10.4	0.70	12.2
				2	140	583	9.6	0.64	11.3
				3	139	586	9.9	0.66	11.6
				4	138	580	9.3	0.63	10.9
				5	139	591	10.7	0.70	12.6
				6	140	592	10.6	0.69	12.4
				7	138	578	8.9	0.60	10.4
				8	139	587	10.1	0.67	11.8

TABLE V. SUMMARY OF INGOT DATA AND CELL CHARACTERISTICS OF BEST CELLS FROM EACH BATCH

Ingot	Crucible	Orientation	Resistivity Ω-cm	Polished Wafers					BSF and/or Texturized				
				AMO I_{sc}	AMO V_{oc}	AMO η	CFF	AM1 η	AMO I_{sc}	AMO V_{oc}	AMO η	CFF	AM1 η
2-021-C	High purity clear	(111)	0.41-0.43	139	618	12.0	0.76	14.1	140	617	12.0	0.75	14.1
2-048-C	High purity graded	(100)	2.4-2.8	133	575	11.2	0.79	13.1	149	591	12.3	0.76	14.4
2-049-C	High purity graded	(100)	3.2-3.7	136	573	11.5	0.80	13.5	156	591	12.8	0.75	15.0
2-050-C	High purity graded	Poly	0.56-0.59	128	599	11.1	0.78	13.0	139	591	10.7	0.70	12.6

TABLE VI. CONVERSION FACTORS FOR CONVERTING AMO INTO AM1 VALUES FOR EACH BATCH TESTED

Ingot	Polished Wafers			BSF and/or Texturized		
	I_{Fac}	V_{Fac}	η_{Fac}	I_{Fac}	V_{Fac}	η_{Fac}
Control	0.873	0.99	1.172			
2-021-C	0.876	0.99	1.173	0.876	0.988	1.171
2-048-C	0.872	0.99	1.168	0.871	0.991	1.168
2-049-C	0.878	0.992	1.178	0.872	0.99	1.168
2-050-C	0.876	0.99	1.172	0.876	0.99	1.173

Process Development

In a short time of about two and a half years, the solar cell efficiency of silicon cast by HEM is up to the efficiency of material produced by the Czochralski method, which has been in production for over two decades. This has been possible by making technological breakthroughs with respect to crucible development, to processing in vacuum, and to heat flow.

One of the crucial problems with casting silicon in silica crucibles is that of ingot cracking. This fundamental problem had been identified as far back as 1949.[4] During Phase I of this program a solution was found with the development of a graded silica crucible. This technical breakthrough was further extended to high purity crucibles during the current program. A typical crackfree ingot as removed from the furnace is shown in Figure 1. There is no cracking on any area of the ingot.

It has been suggested[5] that the reaction between molten silicon and silica crucible to form SiO

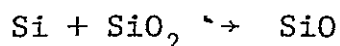

$$Si + SiO_2 \rightarrow SiO$$

would result in decomposition of the crucible. The operation in vacuum would result in acceleration of this reaction. In a motionless process such as HEM, large crystals have been grown in silica crucibles in vacuum without serious deterioration of the crucible.

A basic problem encountered during vacuum operation of silicon crystal growth was the formation of SiC. This has been

ORIGINAL PAGE IS
OF POOR QUALITY

Figure 1. As-cast surface of 6" diameter ingot (#2-041-C)

identified[6] with the reaction of CO and Si

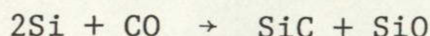

$$2Si + CO \rightarrow SiC + SiO$$

The source of CO, besides a vacuum leak, is associated with the reaction of graphite retainers and silica crucible

$$C + SiO_2 \rightarrow SiO + CO$$

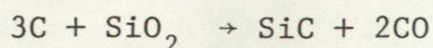

$$3C + SiO_2 \rightarrow SiC + 2CO$$

These reactions became operative, as shown in Figure 2, below about 30 torr near the melting point of silicon. This problem was solved by using molybdenum sheet retainers. A review of data in Table VII shows that the molybdenum sheet reduced the carbon levels in silicon from $(3.5 - 4.1) \times 10^{17}$ atoms/cc (close to solubility limit of carbon in silicon[7]) to $(1.6 - 3.1) \times 10^{17}$ atoms/cc--a reduction of about 50%. SiC associated with high carbon levels floated to the surface of the melt and acted as nucleii for spurious growth. The reduction of such nucleii allowed crystal growth at lower superheat, thereby reducing gradients in the melt. This resulted in better quality crystals as well as better crystallinity.

Operation in a vacuum environment significantly reduced the oxygen concentration in the silicon (Table VII) as compared to a mean value of 25.58×10^{17} atoms/cc reported[8] for Czochralski silicon. The advantage of using a molybdenum retainer further reduced the oxygen levels by acting as a "getter" for oxygen. Operation in vacuum has many advantages. Besides saving the cost

TABLE VII. CORRELATION OF CARBON AND OXYGEN CONTENT IN MELT WITH TYPE OF RETAINER USED

Run #	Retainer Used	Carbon atoms/cc x 10^{17}	Oxygen atoms/cc x 10^{17}
70-C	Graphite	3.71	17.14
109-C	Graphite	3.59	16.9
109-C	Graphite	3.46	15.9
115-C	Graphite	4.07	9.81
115-C	Graphite	4.08	11.76
2-021-C	Molybdenum	2.59	5.78
2-021-C	Molybdenum	2.24	5.58
2-032-C	Molybdenum	1.97	9.57
2-032-C	Molybdenum	1.54	11.4
2-032-C	Molybdenum	2.21	4.19
2-032-C	Molybdenum	3.02	4.54
2-032-C	Molybdenum	2.16	8.96
2-032-C	Molybdenum	3.14	5.24

of high purity argon, heat flow is simplified and higher quality silicon is grown. It has not been possible to grow silicon under vacuum environment, but now it has been demonstrated via the HEM that this can be achieved. By using the technological development described above, operation in vacuum can be extended to other silicon crystal growth and casting operations.

It has been reported[9] that there is a breakdown in crystallinity during Czochralski growth of silicon when the carbon levels are close to solubility limit. By the HEM process, this problem has not been encountered as evidenced in the polished and etched section shown in Figure 3. When SiC is formed it floats to the surface of the melt and does not physically impinge on the growing solid-liquid interface. This makes it possible to grow single crystal ingots from contaminated silicon, since many impurities float to the surface.

Heat extraction in the HEM is via the bottom of the crucible. Since the conductivity through silica is not conducive to heat extraction, a graphite plug was inserted through a hole at the bottom of the crucible. During heat up the reaction of the silicon seed with the graphite plug formed a SiC seal which was leak-proof to molten silicon. Growth rates of 0.75-1.0 kg/hr have been achieved using this approach. At the present time this has not been optimized and higher growth rates are expected.

The best quality and fastest silicon crystal growth from the melt is achieved when the liquid temperature is held close to the

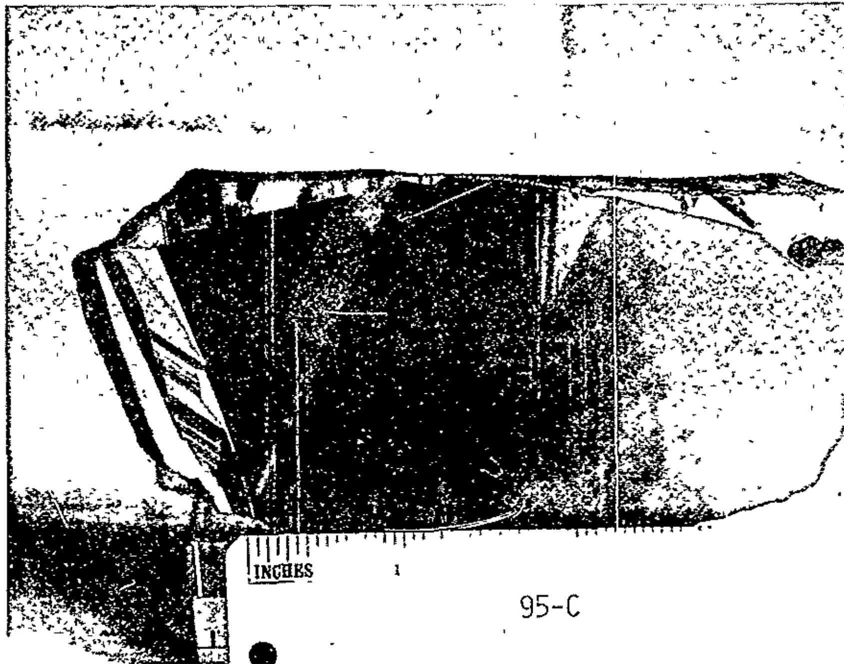

Figure 3. Polished and etched section of run #95-C.

ORIGINAL PAGE IS
OF POOR QUALITY

melting point. As crystal growth by HEM progresses the cooling effect of the heat exchanger cools the furnace and some freezing occurs from the top. A temperature gradient was built in the furnace by designing a new heater. This would allow liquid near the interface to be close to the melting point without freezing occurring at the top surface.

Distribution of dopant during HEM silicon growth is very uniform. A slab from a 3 kg ingot cast in run 2-042-C was examined for resistivity by measuring on a grid pattern and taking five readings at each position. Four-point resistivity data is shown in Table VIII along with the grid pattern in Figure 4. Uniform dopant distribution is probably achieved because HEM growth is motionless directional solidification with minimum convection.

It is well known that solar cell performance is degraded significantly when impurities are incorporated in the silicon. In conventional crystal growth processes, care has to be exercised to avoid contamination of the furnace by using purified graphite parts and high purity crucibles. At the present time the HEM furnace chamber has been constructed from unpurified graphite parts and further contaminated by using low purity grades of silica crucibles. Typical analysis of a graphite part used is given in Table IX. It can be seen that the level of impurities of 728 ppm is rather high which would result in contamination of the furnace. Solar cells fabricated from ingots grown in the

TABLE VIII. FOUR POINT PROBE RESISTIVITY DATA ON SAMPLE FROM 2-042-C. THE POSITIONS ARE AS SHOWN IN FIGURE 4.

Position \ Reading No.	#1	#2	#3	#4	#5
1	0.7 Ω-cm	0.7	0.75	0.75	0.70
2	0.8	0.75	0.75	0.75	0.80
3	0.75	0.75	0.75	0.70	0.75
4	0.75	0.70	0.75	0.75	0.75
5	0.75	0.75	0.75	0.75	0.75
6	0.65	0.65	0.70	0.65	0.65
7	0.65	0.75	0.75	0.65	0.70
8	0.75	0.75	0.75	0.75	0.75
9	0.75	0.75	0.75	0.75	0.75
10	0.70	0.65	0.65	0.70	0.65
11	0.65	0.60	0.65	0.65	0.60
12	0.65	0.65	0.65	0.65	0.65
13	0.70	0.75	0.75	0.75	0.70
14	0.70	0.70	0.75	0.70	0.70
15	0.70	0.70	0.65	0.65	0.65
Seed Area:					
2a	2.4	2.3	2.4	2.4	2.45
2b	1.9	2.0	2.0	-	-
2c	1.2	1.1	1.4	-	-
3a	2.25	2.4	2.45	2.3	2.7
3b	1.0	1.0	1.5	-	-
3c	1.0	1.15	1.25	-	-

ORIGINAL PAGE IS
OF POOR QUALITY

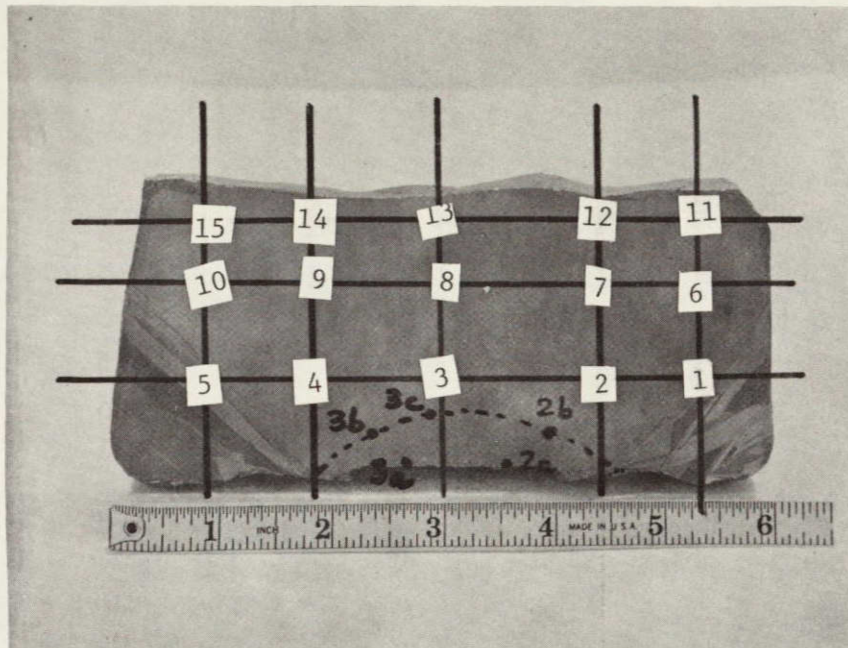

Figure 4. Grid pattern for resistivity measurements.
The numbers indicate positions in Table VIII.

TABLE IX. TYPICAL IMPURITIES OF GRAPHITE USED IN HEM FURNACE MEASURED BY SPECTROGRAPHIC ANALYSIS

Element	Content (ppm)
Mg	13.0
Si	> 100.0
Fe	120.0
Ni	1.0
Al	100.0
Cu	12.0
V	10.0
Ti	23.0
Ca	325.0
Pb	9.0
Cr	5.0
Mo	N.D.*
Mn	$\sim$ 10.0
B	N.D.
TOTAL	> 728.0

*Not detected.

contaminated furnace are nearly state-of-the-art. It is hypothesized that the 0.1 torr vacuum minimizes the effect of volatile impurities.

Even though dislocation densities below 100 per cm^2 have been achieved in HEM silicon[10] the material from run 2-021-C showed 2×10^4 per cm^2 and yet gave a solar cell conversion efficiency of 14% (AM1).

Solar cell conversion efficiency obtained with HEM silicon has been up to 15% (AM1). This has been achieved without optimization of material or cell processing parameters. Improvement in cell performance is expected from casting in an uncontaminated furnace and optimization of material, i.e., defect density, resistivity, and optimization of cell processing parameters, such as diffusion depth, back surface field, texture etch, etc.

CRYSTAL SLICING

Efforts in the area of silicon crystal slicing were continued towards Blade Development, Machine Development and Testing. A big improvement has been achieved in the impregnated wires both in diamond concentration and bladelife. Life and cutting performance of commercially impregnated wires has been related to diamond type. Diamond concentration was controlled with a view to achieve maximum density and impregnating only on the cutting edge thereby reducing the amount of diamond used. Initial tests on the new high-speed slicer have shown that it will meet design specifications.

Blade Development

The best commercially impregnated wires were used in runs 77-S through 79-S[2] and 2-004-S[11]. In these runs good cutting rates and life were achieved. Figure 5 shows the longitudinal and cross-sections of these unused and used wires. It can be seen that some diamonds are still left on the wire even though their concentration is not as high as the unused wires. The cross-section shows that the diamonds have prevented the nickel layer from abrading.

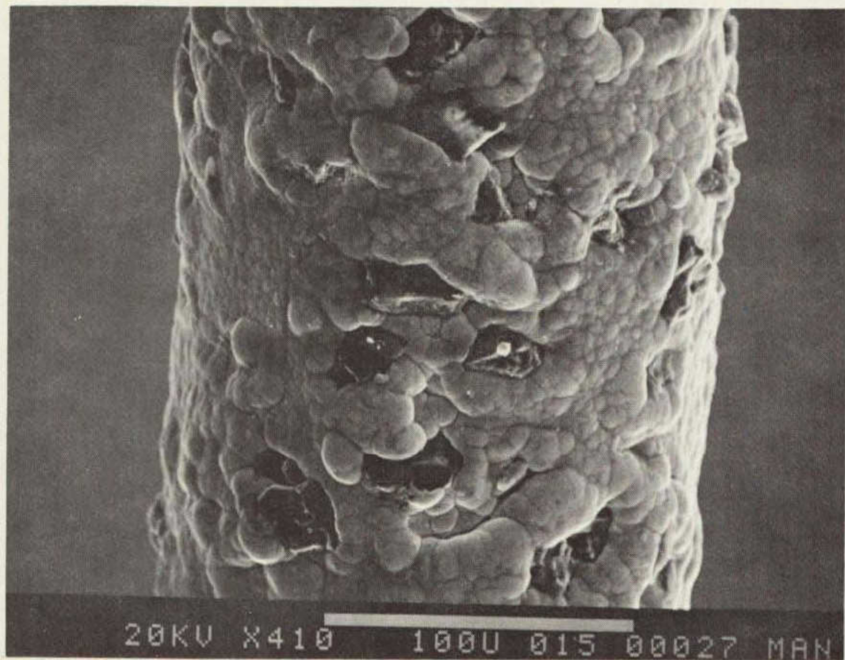

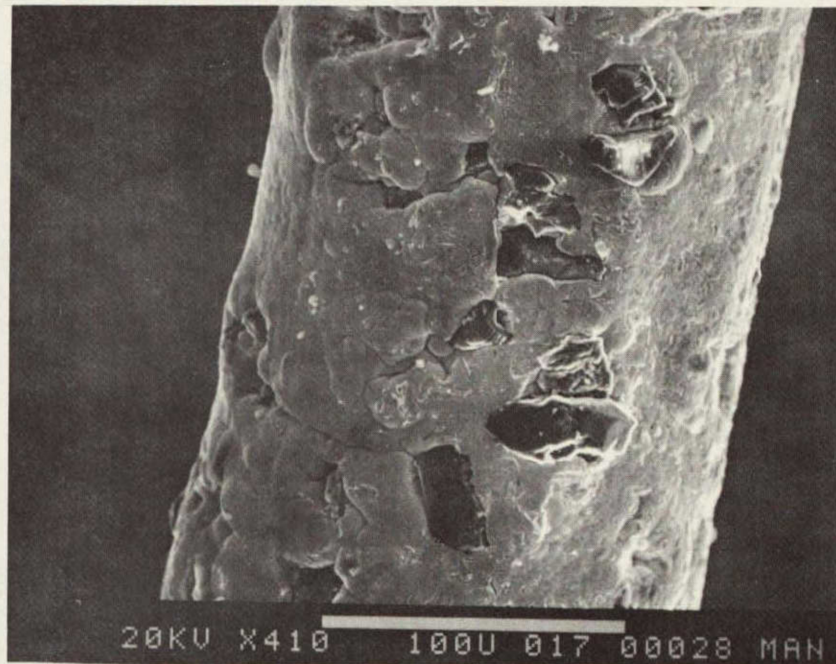

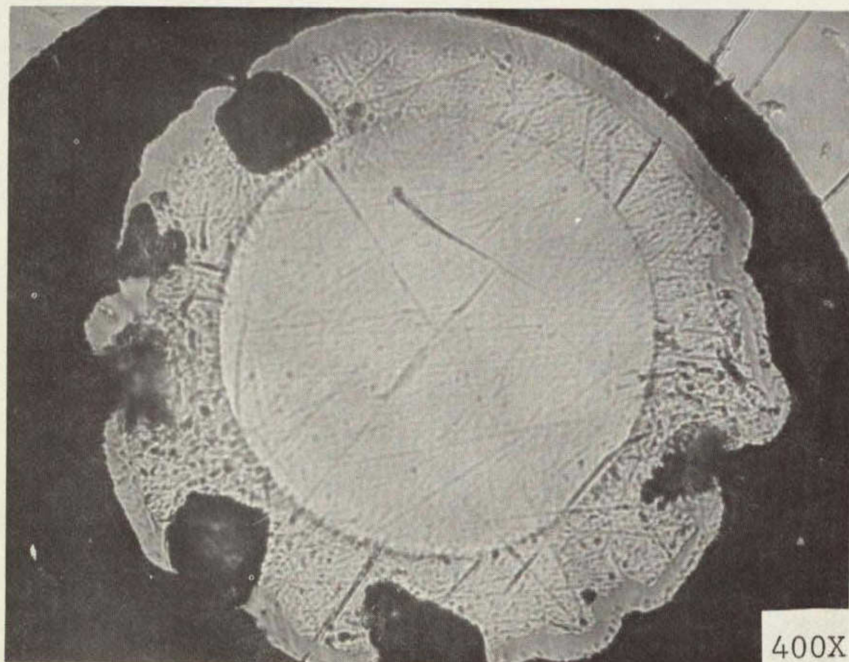

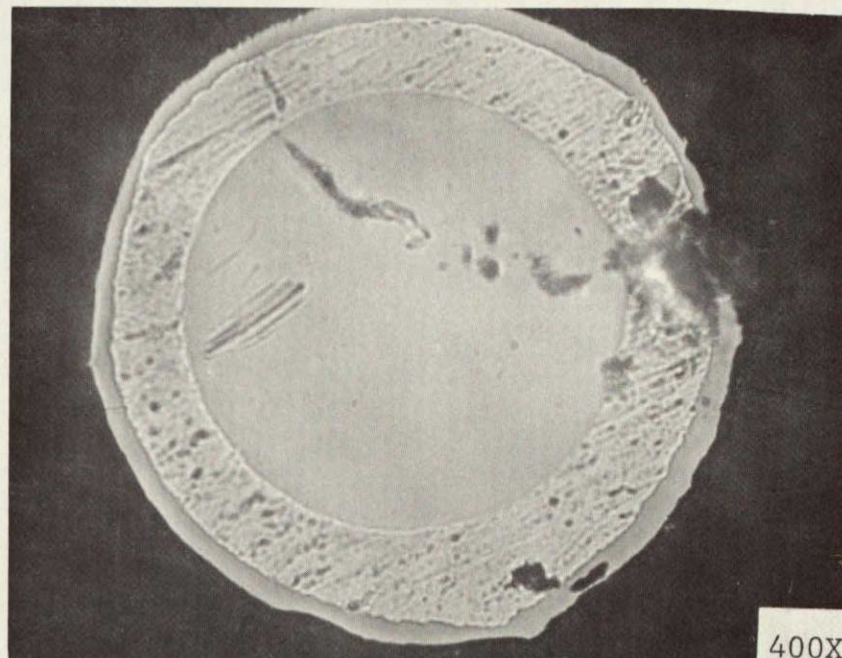

(a) (b)

Figure 5. Impregnated wire 0.3 mil electroless nickel plated (a) unused and (b) used in runs 77-S through 79-S

ORIGINAL PAGE IS OF POOR QUALITY

During recent experiments it was found that this performance could not be duplicated with identical commercially impregnated wire as evidenced in Figure 6. A close examination of the diamonds showed that these diamonds were "blocking" type as compared to sharp edges in earlier wires (Figure 7). This led to the possibility that the recent wires were not identical, but had synthetic diamonds. This could not be confirmed by the manufacturer of the commercially impregnated wire.

To determine the effect of diamond type, wires were manufactured using only natural or only synthetic diamonds. A bladepack was made up from wire impregnated with synthetic diamonds. This wire was double run so that a higher concentration was achieved. The bladepack was electroless nickel plated with 0.3 mil, 7.5 μm and heat-treated at 375°F. These are the conditions which were used in runs 77-S through 79-S. This bladepack was tested in runs 2-048-S and 2-049-S (details in Table X). It was found that good initial cutting rates were obtained but they degraded with the depth of cut indicating diamond pull-out during slicing.

A bladepack made up using single run natural diamond impregnated wire was similarly plated and heat treated. It was used in runs 2-050-S through 2-055-S. The performance of this set of wires is superior to any seen so far using commercially impregnated wires. It can be seen that there is a gradual deterioration in cutting rates. This is attributed to pull-out of diamonds

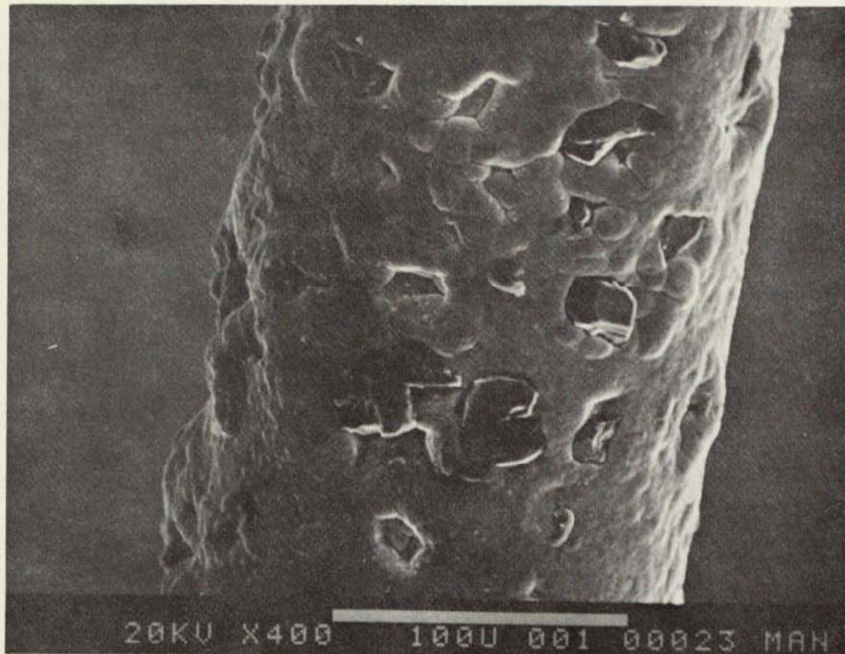

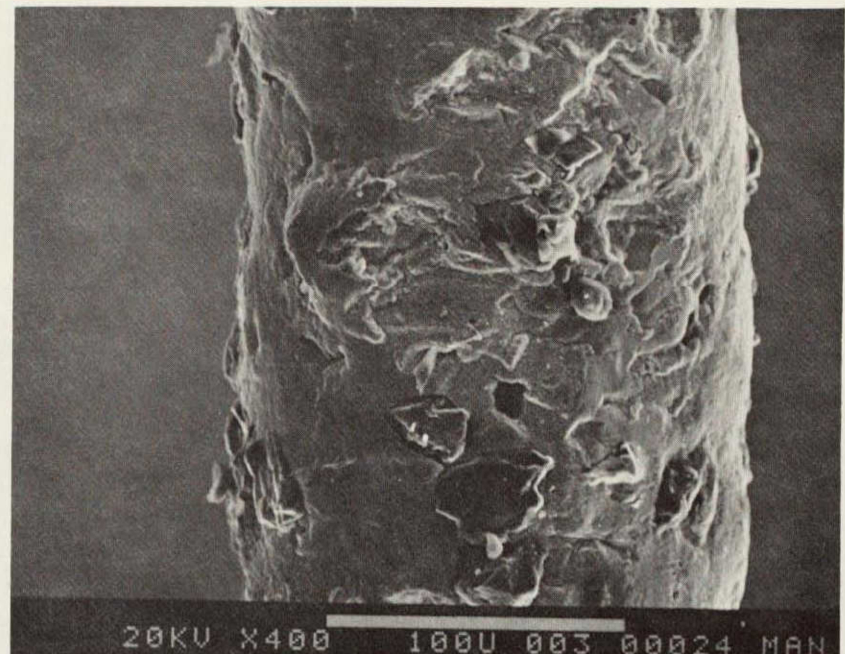

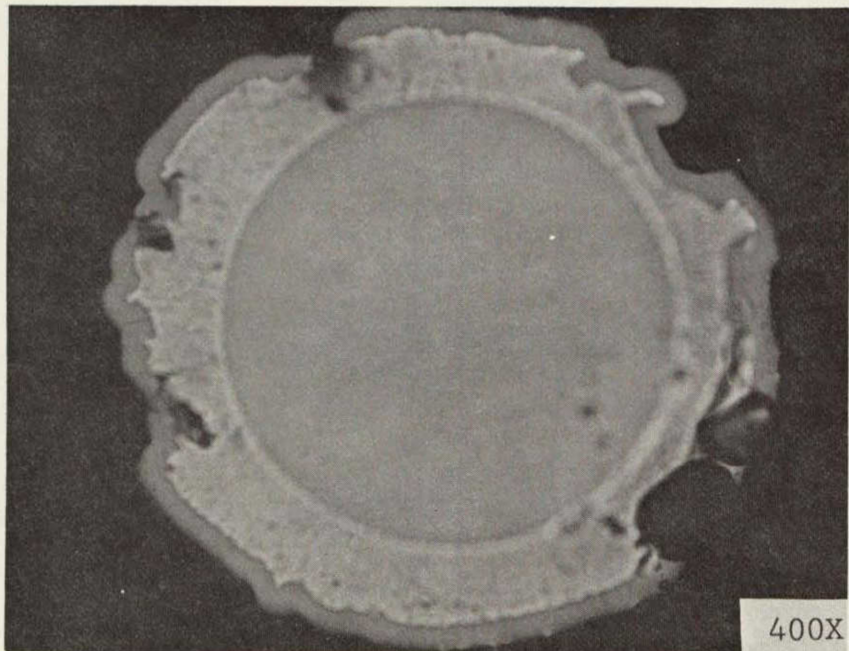

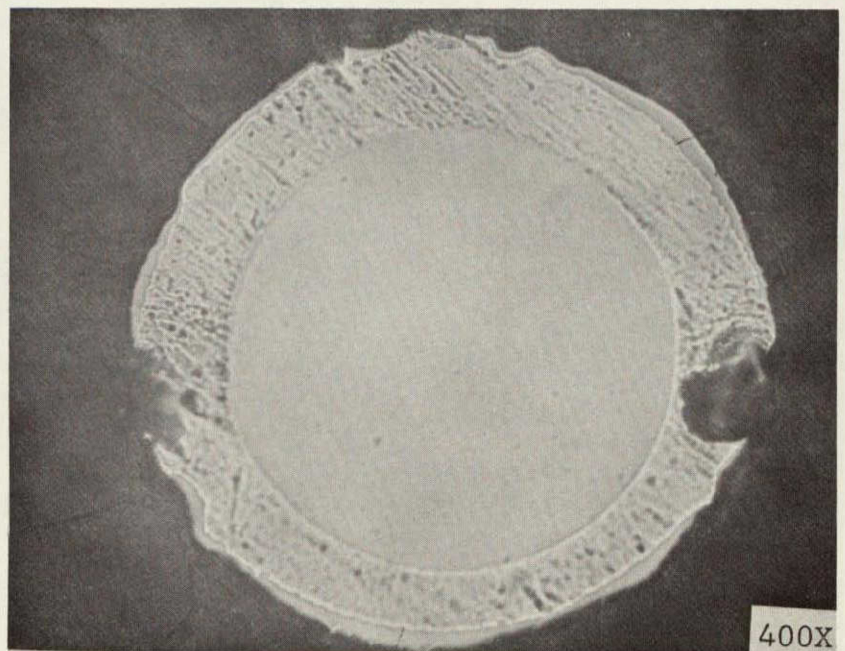

(a) (b)

Figure 6. Impregnated wire 0.3 mil electroless nickel plated (a) unused and (b) after use in runs 2-032-S and 2-033-S

ORIGINAL PAGE IS OF POOR QUALITY

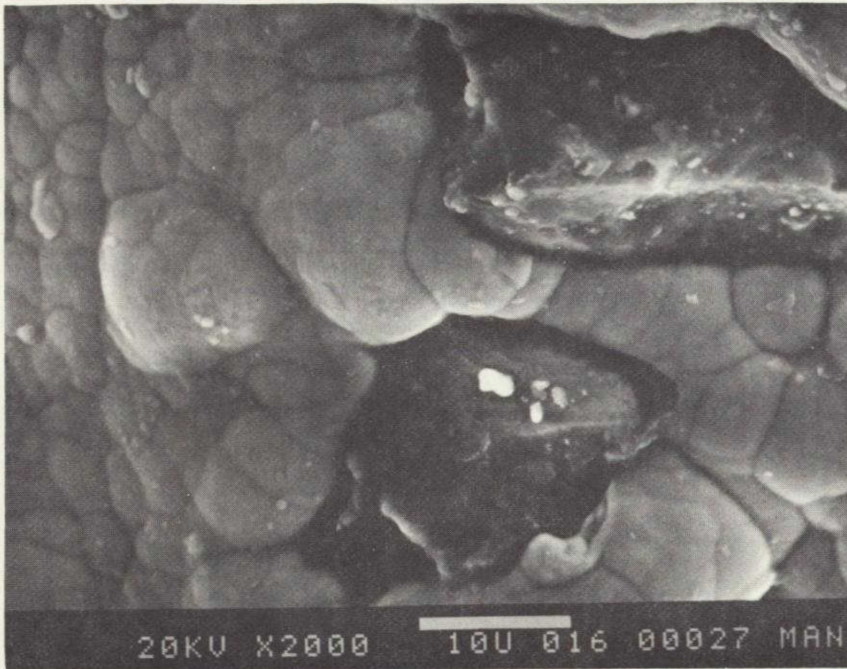

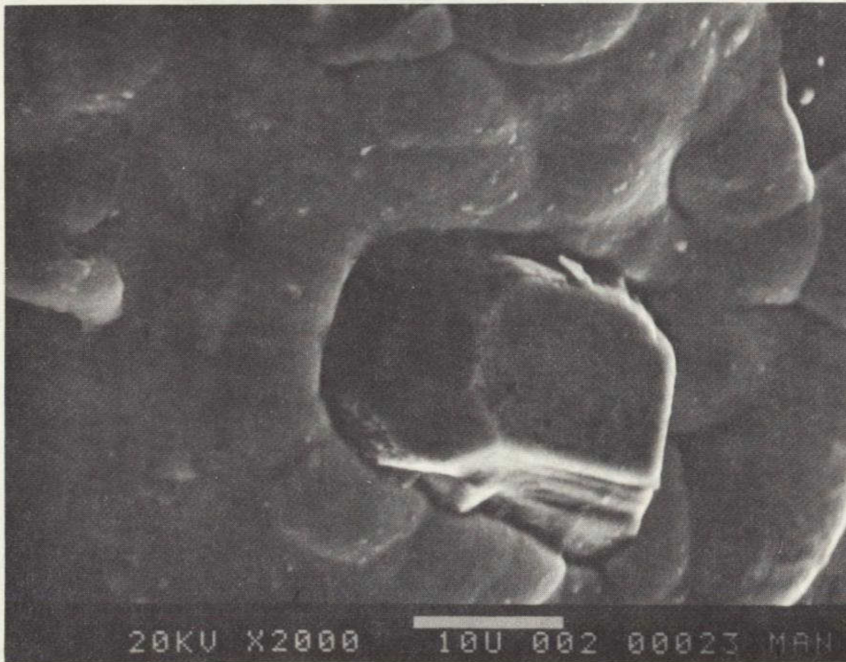

ORIGINAL PAGE IS
OF POOR QUALITY

Figure 7. Examination of diamonds (a) sharp edges--blade used in runs 77-S through 79-S; (b) "blocky"--blade used in runs 2-032-S and 2-033-S.

TABLE X. SILICON SLICING SUMMARY

RUN	PURPOSE	FEED FORCE/BLADE lb.	FEED FORCE/BLADE gm	AVERAGE CUTTING RATE mil/min	AVERAGE CUTTING RATE mm/min	WIRE TYPE	REMARKS
2-038-S	Life test commercially impregnated wire	0.083	37.7	1.60	0.040	Commercial 8 mil, 0.2 mm core impregnated with 45 µm diamond; 0.3 mil, 7.5 µm electroless nickel plated; 375°F heat treated	Fair cutting rates and wafer quality.
2-039-S	Life test	0.083	37.7	1.38	0.035	Same as 2-038-S	Fair wafer quality
2-040-S	Life test	-	-	-	-	Same as 2-038-S	Run aborted due to poor cutting rates
2-041-S	Life test CSI impregnated wire	0.075	34.4	1.50	0.038	5 mil, 0.125 tungsten core; 0.3 mil, 7.5 µm copper sheath; CSI impregnation with nickel clad diamond; 0.5 mil, 12.5 µm electroless nickel plated	Good initial cutting rates, yield 77%
2-042-S	Life test commercially impregnated wire using harder plating	0.080	36.3	2.70	0.068	Commercial 8 mil, 0.2 mm core impregnated with 45 µm diamond; 0.3 mil, 7.5 µm harder nickel plating; no heat treatment	Good cutting rates. Very good wafer quality.
2-043-S	Life test	0.080	36.3	1.65	0.041	Same as 2-042-S	Very good wafer quality.
2-044-S	Life test	0.080	36.3	1.22	0.031	Same as 2-042-S	Good wafer quality.

TABLE X. (Cont.)

RUN	PURPOSE	FEED FORCE/BLADE lb	FEED FORCE/BLADE gm	AVERAGE CUTTING RATE mil/min	AVERAGE CUTTING RATE mm/min	WIRE TYPE	REMARKS
2-045-S	Reduce kerf.	N/A	N/A	N/A	N/A	5 mil, 0.125 mm tungsten core; 0.3 mil, 7.5 µm copper sheath; 45 µm diamond CSI impregnation. 0.6 mil, 15 µm electroless nickel plated	Run aborted due to wire breakage caused by insufficient clearance by diamonds
2-046-S	Reduce kerf.	0.075	34.1	1.60	0.040	5 mil, 0.125 mm tungsten core; 0.5 mil, 12.5 µm copper sheath; 45 µm diamond CSI impregnation. 0.5 mil, 12.5 µm electroless nickel plated	Good quality wafers.
2-047-S	Life test.	N/A	N/A	N/A	N/A	Same as 2-046-S	Run aborted due to wire breakage because of diamond pull-out.
2-048-S	Test synthetic diamond	0.080	36.3	2.75	0.070	Commercial 45 µm synthetic diamond impregnated wire (double run); 0.3 mil, 7.5 µm electroless nickel plating; 375°F heat treated	Good cutting rates; low yields.
2-049-S	Life test	0.080	36.3	1.32	0.034	Same as 2-048-S	Fair cutting rates; poor yields.

TABLE X. (Cont.)

RUN	PURPOSE	FEED FORCE/BLADE		AVERAGE CUTTING RATE		WIRE TYPE	REMARKS
		lb	gm	mil/min	mm/min		
2-050-S	Test natural diamonds	0.088	40.0	3.30	0.083	Commercial 45 μm natural diamond impregnated wire; 0.3 mil, 7.5 μm electroless nickel plating; 375°F heat treatment.	Good cutting rates; poor yield - 40%.
2-051-S	Life test continuation	0.082	37.1	2.56	0.065	Same as 2-050-S.	Good cutting rates; 85% yield.
2-052-S	Life test continuation	0.075	34.3	1.96	0.050	Same as 2-050-S.	Very good wafer quality; 85% yield.
2-053-S	Life test continuation	0.075	34.3	1.76	0.048	Same as 2-050-S.	Very good wafer quality; 89% yield.
2-054-S	Life test continuation	0.075	34.3	1.48	0.037	Same as 2-050-S.	Very good wafer quality; 89% yield.
2-055-S	Life test continuation	0.076	34.8	1.27	0.032	Same as 2-050-S.	Low cutting rates; Poor yield - 65%.

during slicing.

The major problem with impregnated wires is diamond pull-out. It has been demonstrated that it can be prevented by nickel plating after impregnation. It was felt that the bond between the diamond and nickel plating would be improved if the diamonds are clad with nickel. With this in view, nickel was evaporated on diamonds and then impregnated into a copper sheath. Only a low concentration of diamonds were impregnated into the copper sheath. This bladepack, after nickel plating, was used in run 2-041-S. The unused and used sections of a wire using this technique are shown in Figure 8. It can be seen that since the diamonds are clad with nickel, no diamonds are visible in the unused section. The concentration of the exposed diamonds on the used wire is not high due to poor impregnation.

The life tests have shown that the impregnated wires have a shorter life as compared to the electroplated wires. This is probably due to lower concentration of diamonds which results from insufficient suspension of diamonds during impregnation. Recently the viscosity of the suspension medium was increased so that the diamonds were held in suspension. Impregnation carried out using this medium has resulted in diamond concentrations comparable to electroplated wires.

So far the emphasis on the core material has been on tungsten. One of the other candidates for high strength core is

ORIGINAL PAGE IS
OF POOR QUALITY

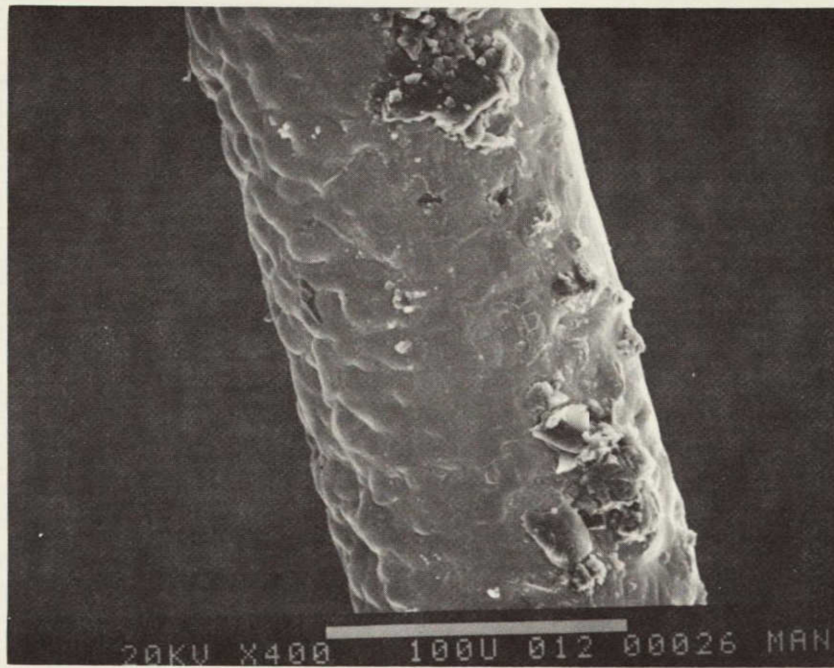

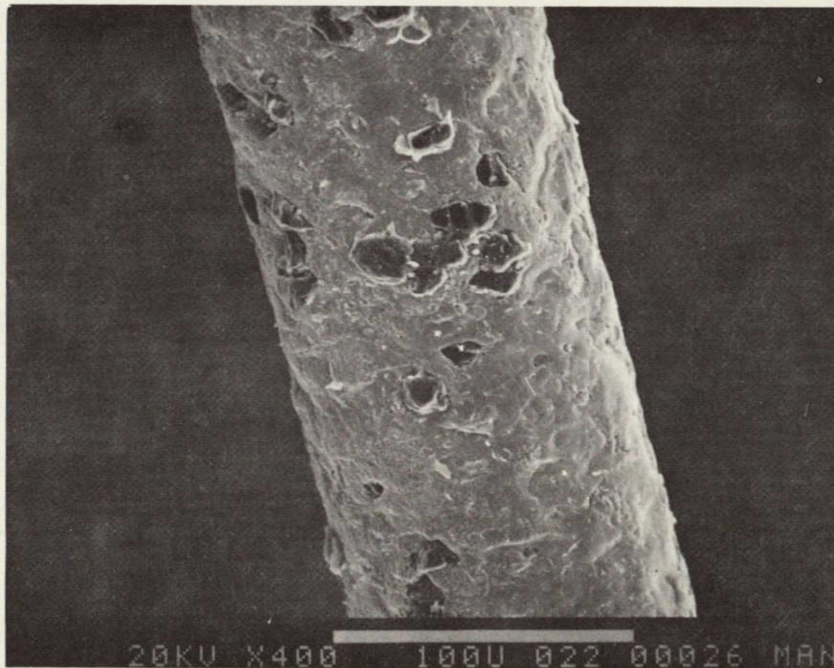

Figure 8. Section of unused and used wire using nickel clad diamond impregnation and plated to prevent diamond pullout (run 2-041-S)

music wire.[2] A sample of this wire was sent to a vendor for electroplating diamonds. SEM examination of two longitudinal and cross-sections of this wire are shown in Figure 9. It can been seen that a very high concentration of the diamonds has been achieved and that enough diamonds are projecting from the plating, hence, available for efficient slicing. Electroplating diamonds on steel core wire by this technique does not present problems. In the past some hydrogen embrittlement has been encountered with steel core plating. No suggestion of such problems is evident in this sample.

In the cleaning procedures prior to plating, acids are used which attack the core wire. Care has to be exercised during this step so that good cleaning is achieved without too much attack on the wire. In order to insure that good cleaning was carried out, it is felt that a metal flash on the core will prevent corrosive attack, as well as serve as a substrate for subsequent nickel plating. Copper and also nickel was flashed on a tungsten core. These wires were then electroplated with diamonds and nickel. Figure 10 shows two longitudinal and two cross-section views of diamond electroplated wire on copper flashed tungsten core. The longitudinal views show that electroplating of diamonds has been achieved to a high concentration. However, some corrosion occurred at the core. Similar examination of diamond electroplated wire on nickel-flashed tungsten core (Figure 11) shows again a high concen-

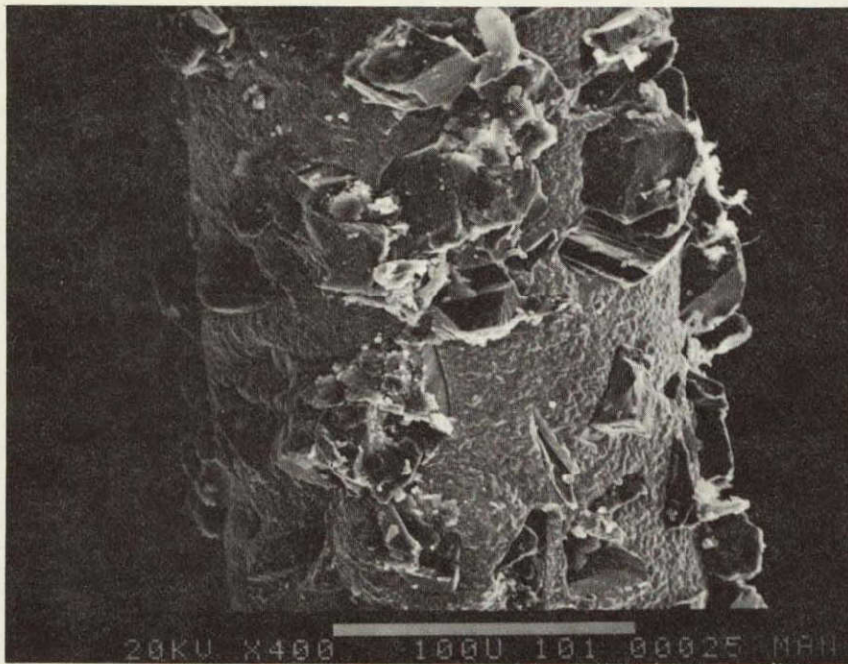

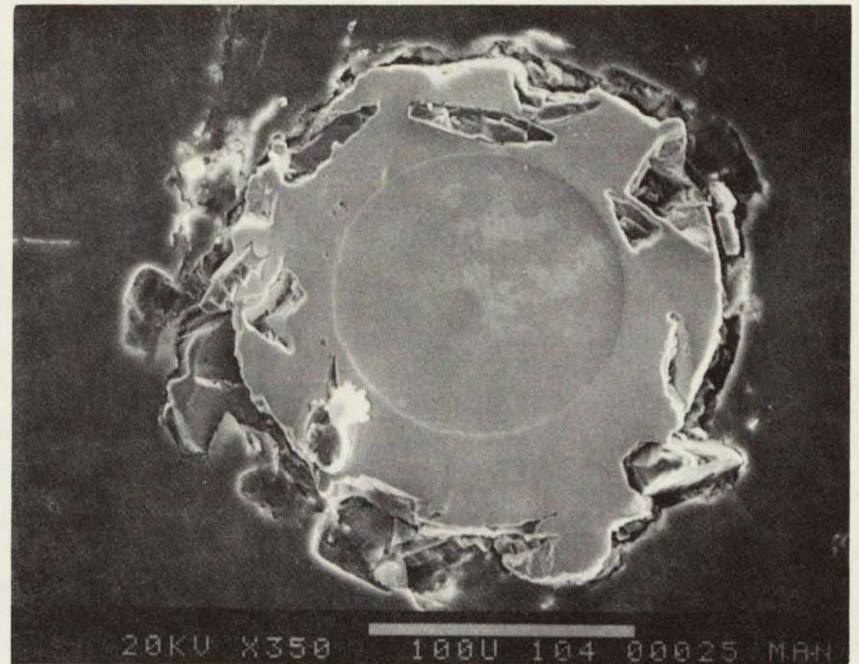

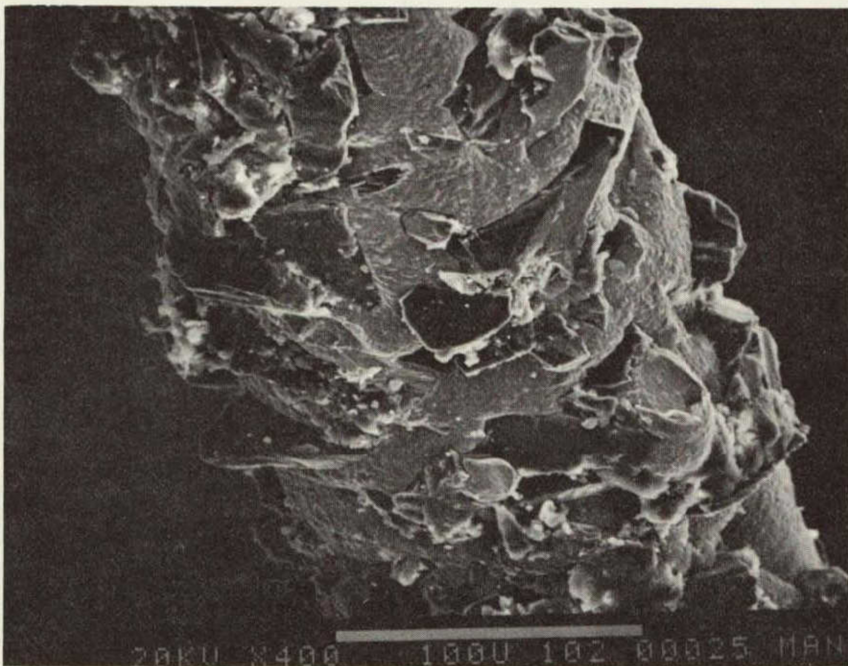

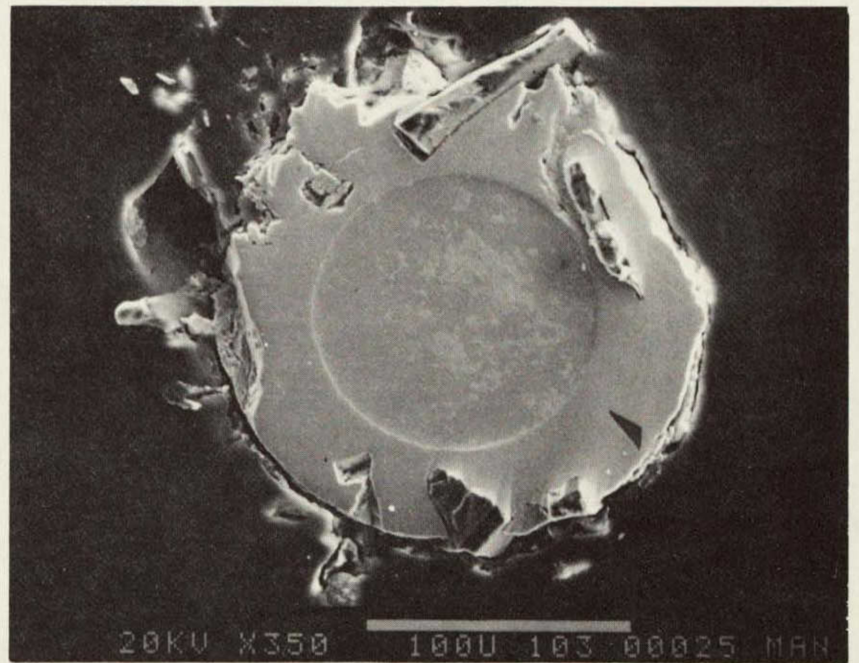

Figure 9. SEM Examination of Electroplated Diamond Wire Using Stainless Steel Core

ORIGINAL PAGE IS
OF POOR QUALITY

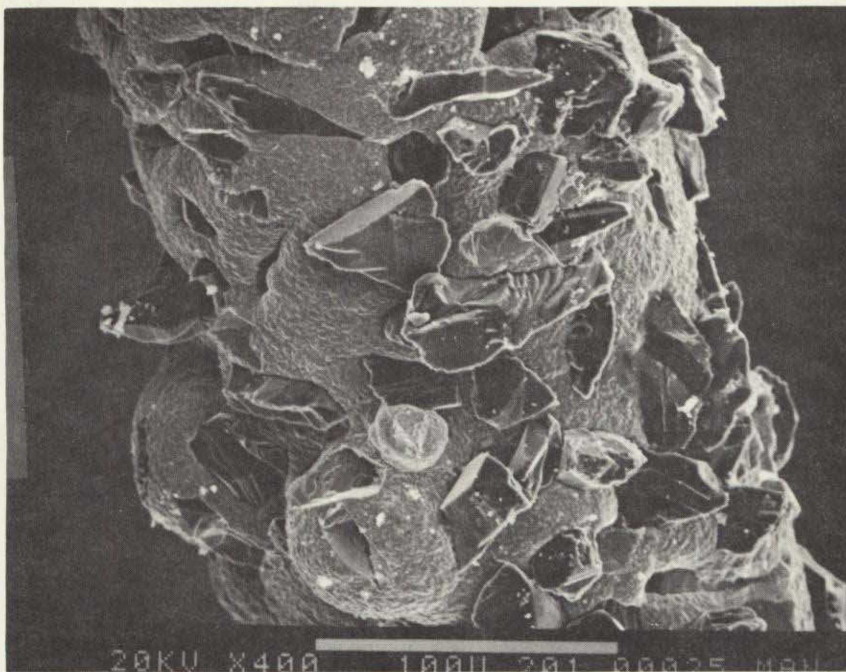

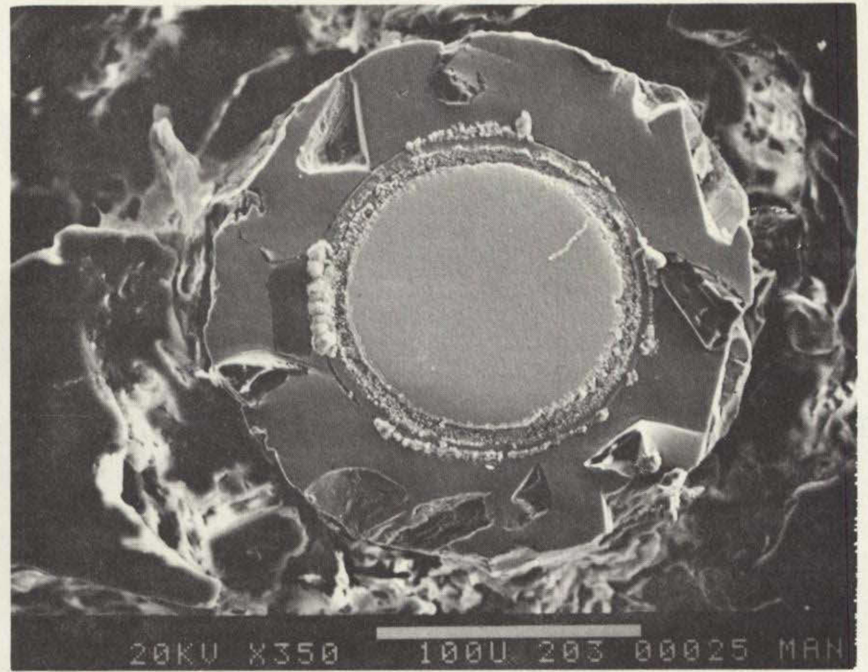

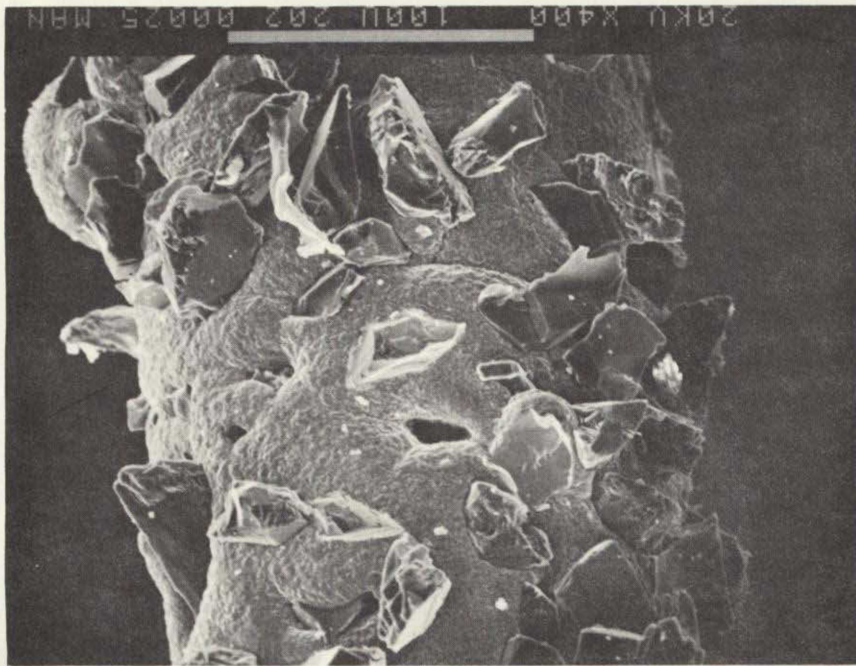

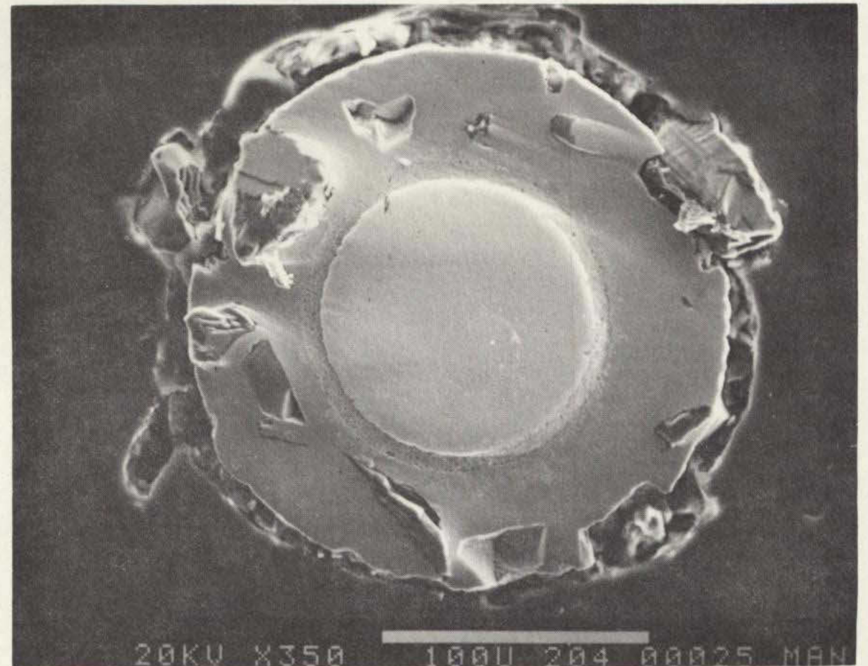

Figure 10. SEM Examination of Electroplated Diamond Wire using Copper Flash, Tungsten Core

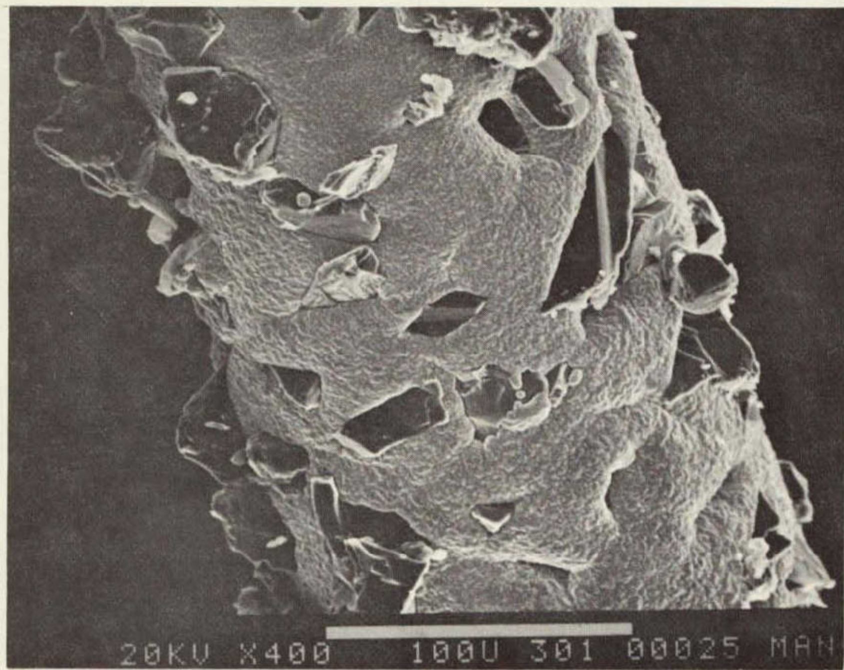

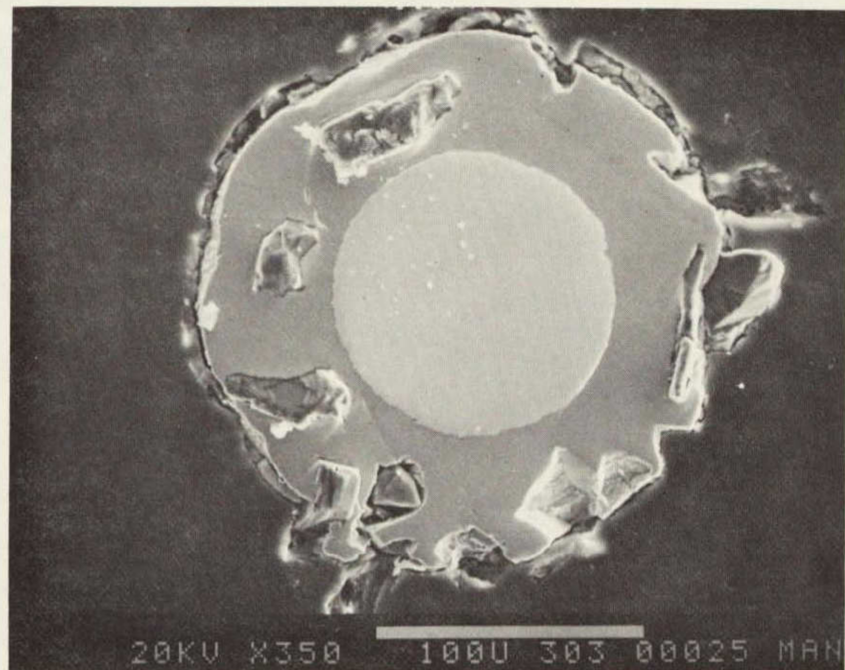

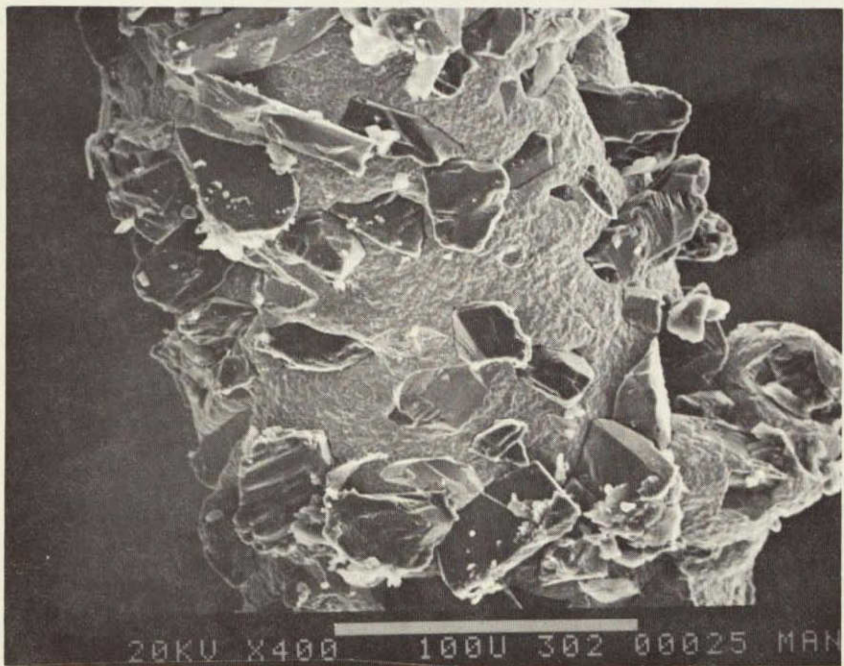

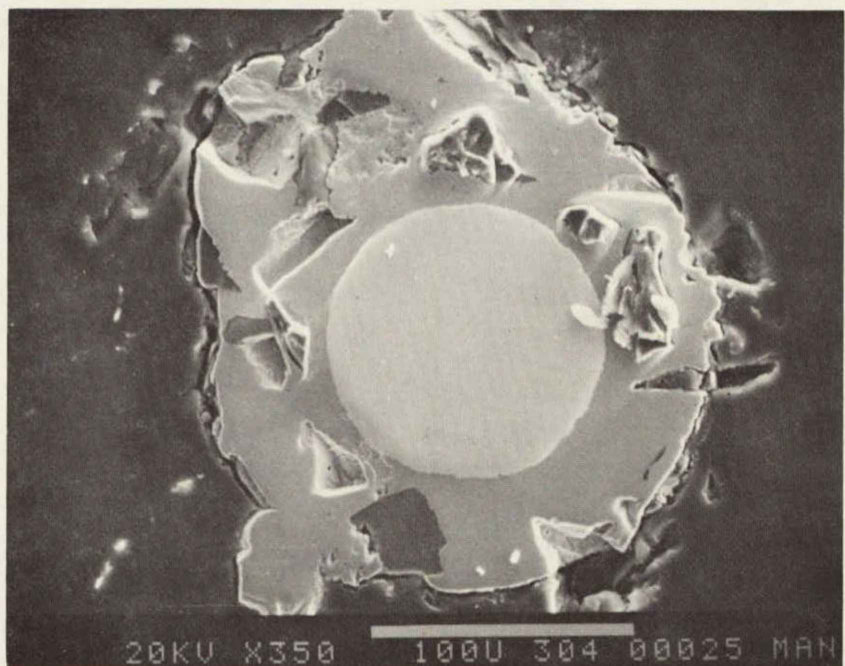

Figure 11. SEM Examination of Electroplated Diamond Wire Using Nickel Flash, Tungsten Core

ORIGINAL PAGE IS
OF POOR QUALITY

tration of diamonds but no corrosion problems at the core.

Efforts to Reduce Kerf

Lower kerf is achievable with impregnated wires. The commercially impregnated wires give a kerf of about 9 mils, 0.225 mm. Crystal Systems impregnation technology allows a lower kerf and it has been reduced to 6.2 mils, 0.155 mm. [2] This was achieved by impregnating diamonds only in the cutting edge. Besides using less diamonds these wires do not degrade the support rollers. In an effort to reduce kerf further, it has been demonstrated[1] that 45 μm diamonds can be impregnated into a 0.3 mil, 7.5 μm copper sheath. For run 2-045-S (details in Table X) a set of wires with 0.3 mil, 7.5 μm copper sheath were impregnated with 45 μm diamonds. The impregnation was limited to less than half the circumference of the wires. These wires were plated with 0.6 mil, 15 μm nickel. During testing it was found that wire breakage occurred which may be due to lack of diamonds on the sides to clear the wires or insufficient thickness of copper and nickel to hold the diamonds. For run 2-046-S, 45 μm diamonds were impregnated into 0.5 mil, 12.5 μm copper sheath to a bigger circumference coverage than the earlier experiment. The wires were plated with 0.5 mil, 12.5 μm nickel. During testing in run 2-046-S good quality wafers were sliced; however, in the subsequent run (2-047-S) significant diamond pull-out occurred. Calculations show that the plating plus sheath thickness corresponds to about

55% of the maximum diamond dimension.

The commercially available impregnated wire has a 5 mil core, 1.5 mil copper sheath into which 45 μm diamonds are impregnated. After impregnation, this leaves only 7.5 μm of the maximum length of diamond exposed. A 7.5 μm nickel plating is necessary to prevent diamond pull-out. Therefore only those diamonds are exposed which are not impregnated fully to the core. Therefore, the diamond concentration after plating is low.

Using Crystal Systems impregnation methods it has been shown that 45 μm diamonds can be impregnated into a 7.5 μm copper sheath --leaving enough thickness for plating to hold the diamond and still leave it exposed for slicing. Figure 12 shows a cross-section of two wires in which 45 μm diamonds were impregnated into a 7.5 μm copper sheath. It can be seen that the thin copper sheath is deformed during impregnation. The diamonds are pushed into the bottom cutting edge only and the pressure results in an opening on the sides between the tungsten and the copper. Similar impregnation into 12.5 μm and 17.5 μm copper sheaths did not show any deformation of copper (Figure 13). These wires after impregnation were electroless nickel plated and it was seen that the plating, which is normally very uniform for commercially impregnated wire, was concentrated on the side where dimaonds were impregnated (Figure 14). Figure 15 shows a similar result for a 17.5 μm copper sheath wire cross-section with Edax counts showing copper and nickel distribution. This was a little surprising; however,

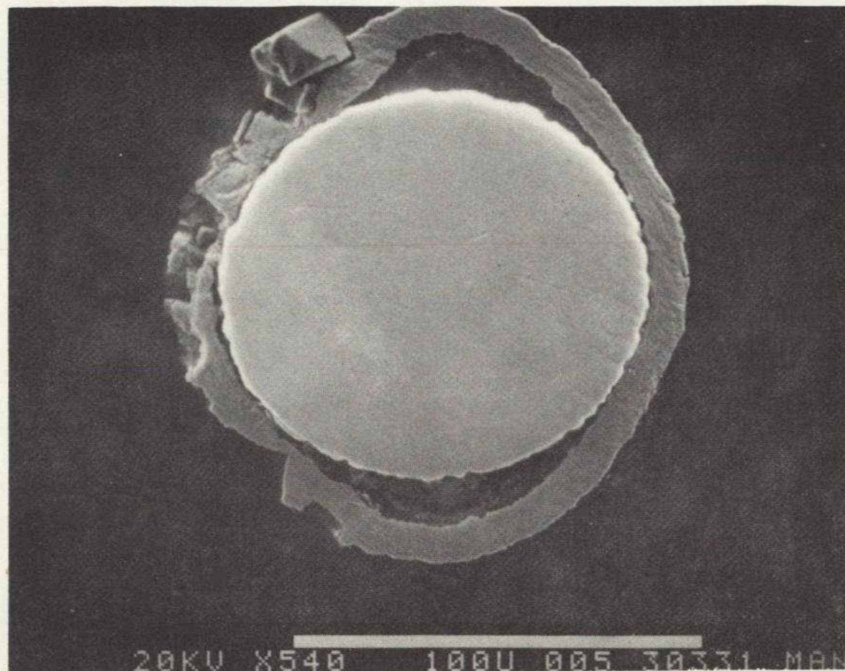

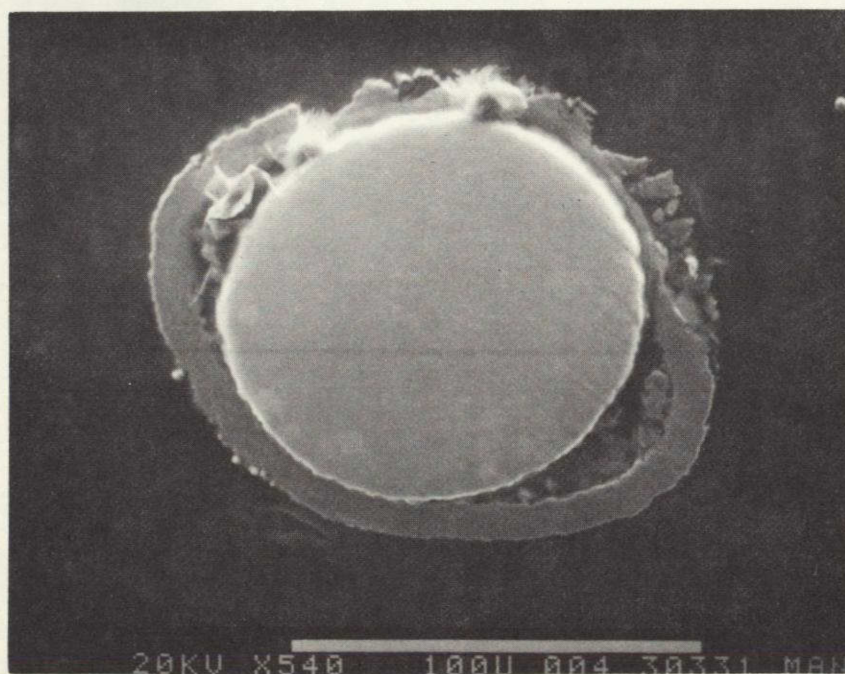

Figure 12. Cross-section of wires impregnated with 45 μm diamonds into 7.5 μm copper sheath showing deformation of copper

ORIGINAL PAGE IS
OF POOR QUALITY

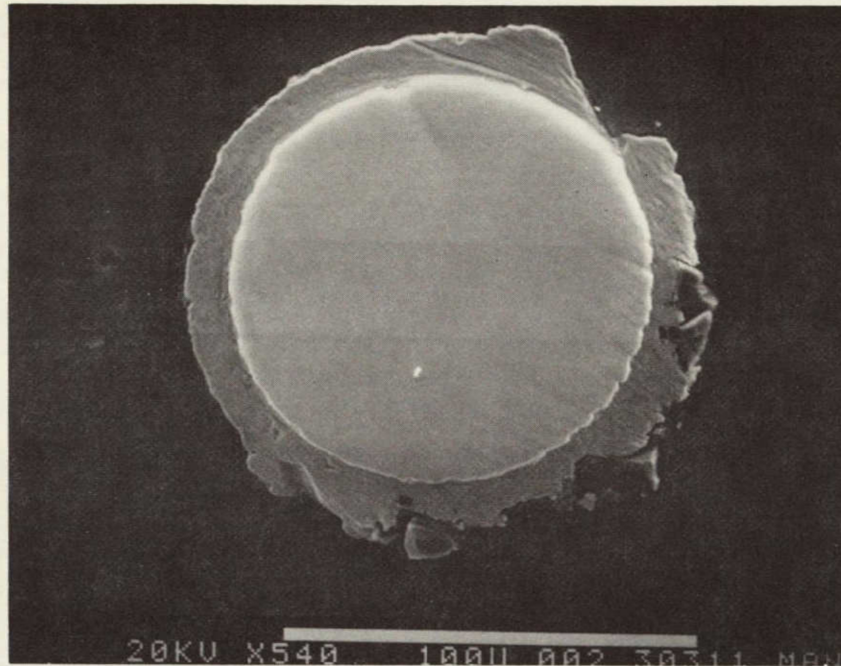

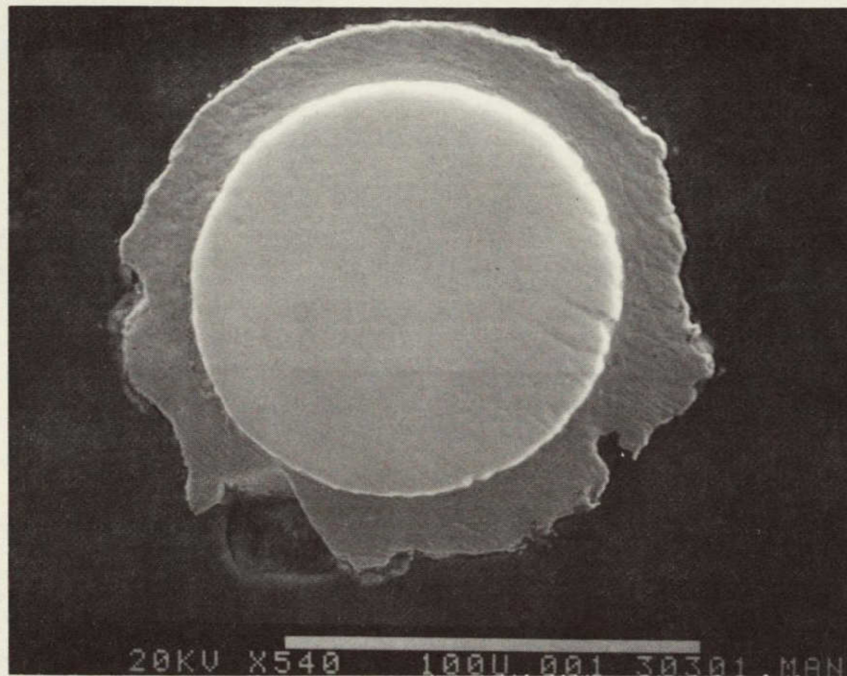

Figure 13. Cross-section of wires impregnated with 45 μm diamonds into (a) 12.5 μm and (b) 17.5 μm copper sheath

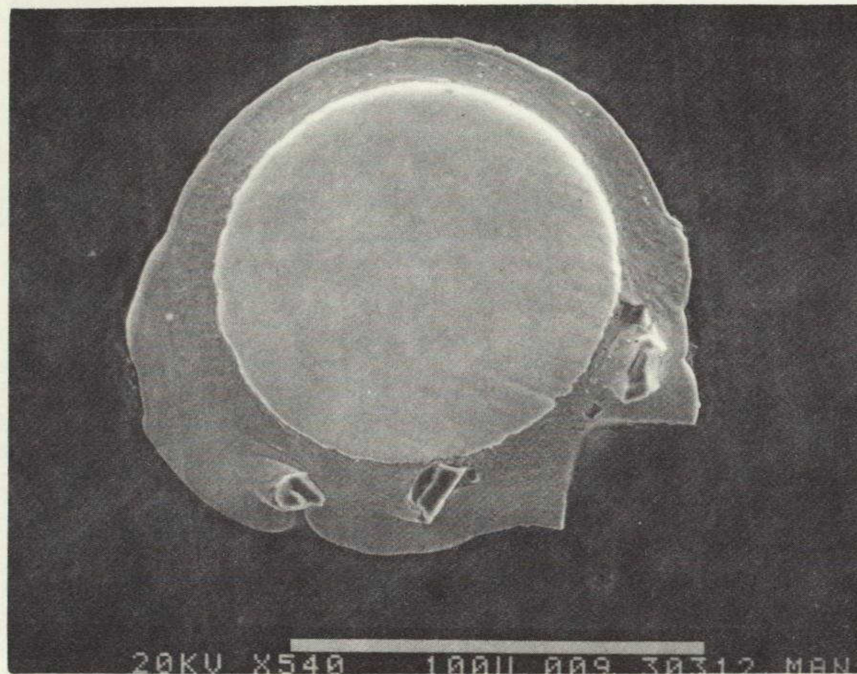

Figure 14. Cross-section of a wire showing that the electroless nickel plating is concentrated in an area of diamond concentration

Figure 15. Cross-sections of electroless nickel plated diamond impregnated wire showing copper and nickel distribution

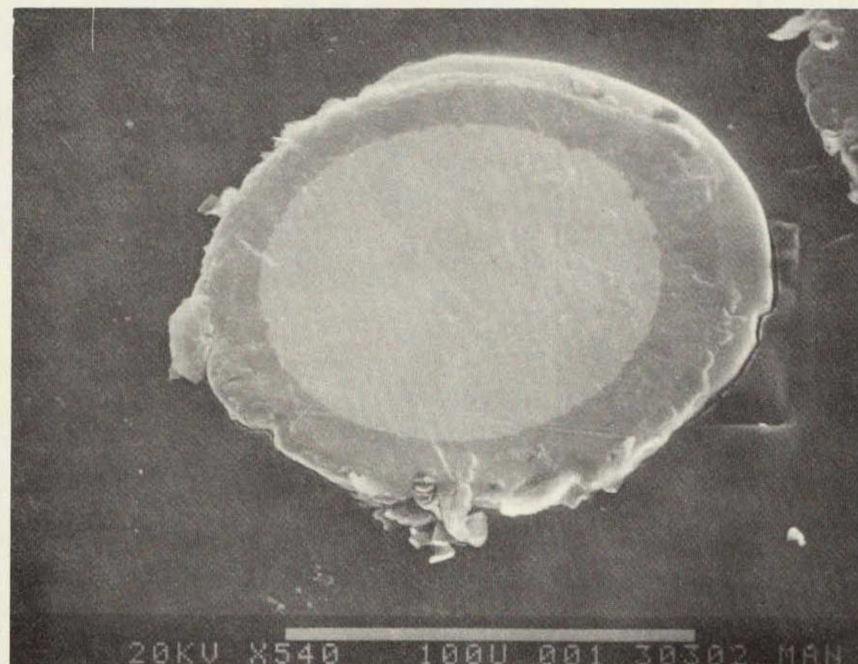

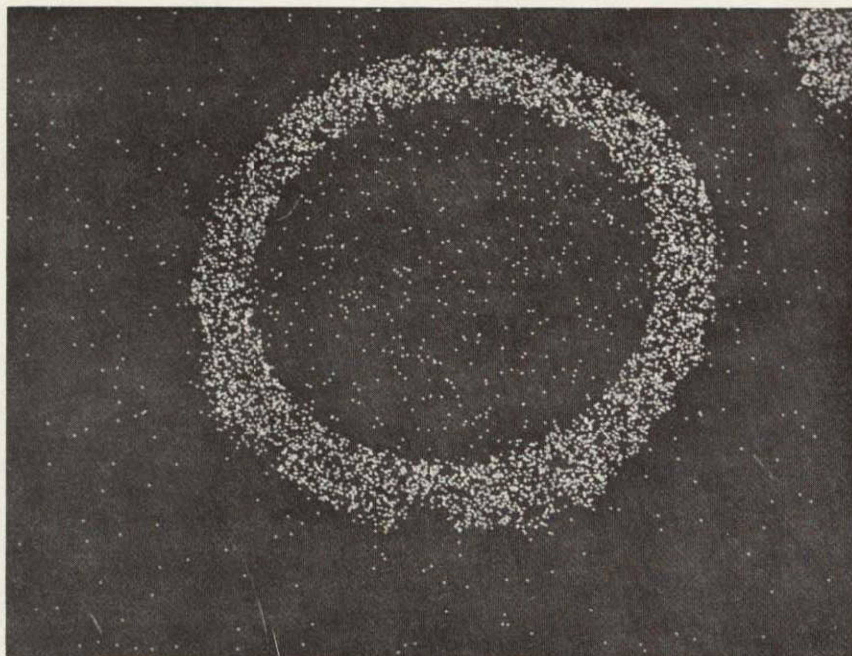

See 30302 : Wire 30B   Copper Distribution

ORIGINAL PAGE IS
OF POOR QUALITY

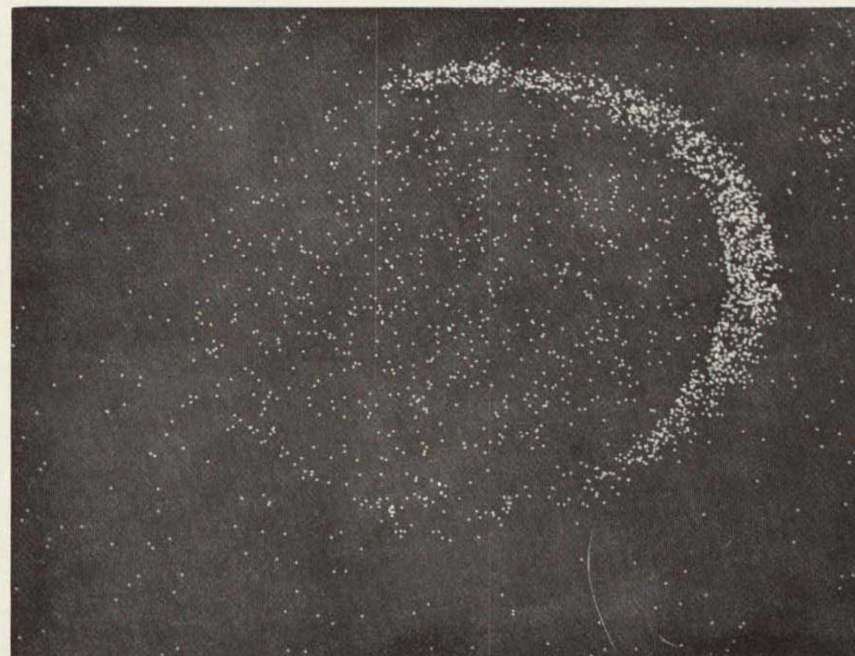

See 30302: Wire 30 B   Nickel Distribution

it can be used to advantage to control kerf. In calculations to reduce kerf it was assumed that nickel will be uniformly plated and will add to the kerf width. As seen in Figure 14, if the nickel will concentrate on the diamonds and they are only in the bottom, the nickel plating will not add to the kerf.

Machine Development

The new high speed slicer has been fabricated and assembled to designed specification. Initial debugging of the machine was carried out with a blade carriage which is about 100 pounds weight as compared to the present machine carriage of 200 pounds. The new bladehead is lighter even though it is twice as long. Tests were carried out without a bladepack, workpiece or counter-balanced weight and a surface speed of 300 ft/min with a 13-inch stroke length was achieved free of vibration. The air bearings, drive mechanism, and isolation of the drive unit seem to be showing a big improvement.

The key to any slicing is in the blade. So far the best blades have shown a lifetime of cutting 22 workpieces of 4 cm x 4 cm size. Even though the cutting rates have averaged about 0.1 mm/min, the life of these blades amounts to about 147 hours. Comparably a typical ID blade cuts a 3-inch workpiece at 1 inch/min for approximately 3000 slices--a life of 150 hours. Thus the life of fixed abrasive wire is comparable to ID blade. It is expected that higher surface speed and larger stroke length available with

materials costs are low as in ID slicing and capital equipment, labor costs are low as in MBS slicing, and material utilization is high as in MWS.

Aside from the economic advantages of the process, there are technical advantages of using multi-wire FAST approach:

a) Wires can be pretensioned to higher stresses.

b) Uniform tensioning of all blades is achieved.

c) Equal spacing of wires is no problem.

d) The diamonds on the wire prevent wire wear; hence, stripping of the wire is not necessary.

e) Wires do not buckle under high feed forces.

f) Due to the symmetry, wires do not torque the wafers after slicing as flat blades.

g) Wires are cheap to fabricate.

h) No fatigue problems because wire is not wrapped around rollers.

i) No corrosion problems since the wires are plated with nickel or copper.

j) In case of wire breakage only two wafers are lost.

Some of the achievements of silicon crystal slicing using the multi-wire FAST approach are:

(i) Machine Development

The slicer used for the FAST approach was one commercially available for MBS method. Extensive modifications were made with the machine to adapt for FAST. Among the first changes made was the feed mechanism. Since very low feed forces

are required for multi-wire slicing a more responsive feed mechanism was designed and fabricated. Cutting tests with fixed diamond at low speeds showed that the workpiece has to be rocked to reduce the kerf length. The necessity for guide rollers was soon evident to minimize wire wander and for effective cutting. Even though major modifications were made with the slicer, certain inherent features of the machine could not be changed. With the limited data available, it was established that higher surface speed, larger rocking angle and longer stroke length will make significant advances in the cutting effectiveness. The present drive mechanisms for the head and rocking fixtures are crank motions which could not be suitably modified and therefore a new high speed machine was designed.

The wire carriage is an aluminum weldment that is reciprocated on air bearings. A wire blade pack is bolted into the carriage and optically aligned. The carriage is moved back and forth by a link guided by a straight line motion mechanism which is crank actuated. By shifting the crank pin location on the guide mechanism, different stroke lengths can be obtained. Beneath the guide mechanism is a second crank which has a mass equal to the carriage weight attached to its end. This crank is driven out of phase with the carriage motion, and thus serves to damp the inertial loads of the system. The sinusoidal crank drive mechanism has been adapted to the output cranks to provide equivalent accelerations at each end of the stroke. In production another carriage will replace the equal mass so two carriages

will be driven by one drive system.

The counterbalanced drive arrangement is mounted on its own plate and shock isolated from the machine frame. The arrangement should radically reduce vibration to the feed mechanism and the crystal mounting. The crystal mount is attached to an air/oil cylinder-driven rocking assembly which attaches to a roller slide mounted to a bracket on the back of the rail support plate. At the present time the parts have been fabricated to the designed specifications and assembly is complete. The machine is currently being debugged.

(ii) Blade Development

The key to slicing by any technique is in the blade; hence strong emphasis has been placed in this area. Basically two types of fixed abrasive wire blades have been developed, viz. diamond electroplated wires (wires plated directly with diamonds) and diamond impregnated wires (wires impregnated with diamonds). Initially diamond electroplated wires were used. Techniques were developed to achieve a very high concentration of diamonds with good uniformity. An SEM photograph of a typical wire is shown in Figure 16. Such blades were used to slice up to 22 workpieces of 4 cm x 4 cm size. Even though these blades gave a good cutting performance and life, the kerf could not be controlled below about 8 mil, 0.2mm.

The diamond impregnated wires were also tested. Commercially available wires suffered from diamond pull-out,

ORIGINAL PAGE IS
OF POOR QUALITY

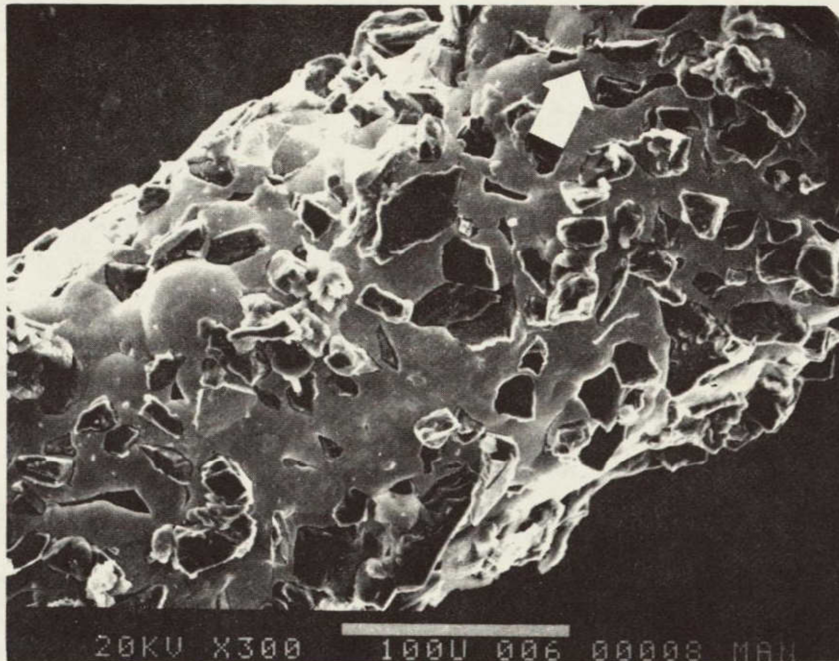

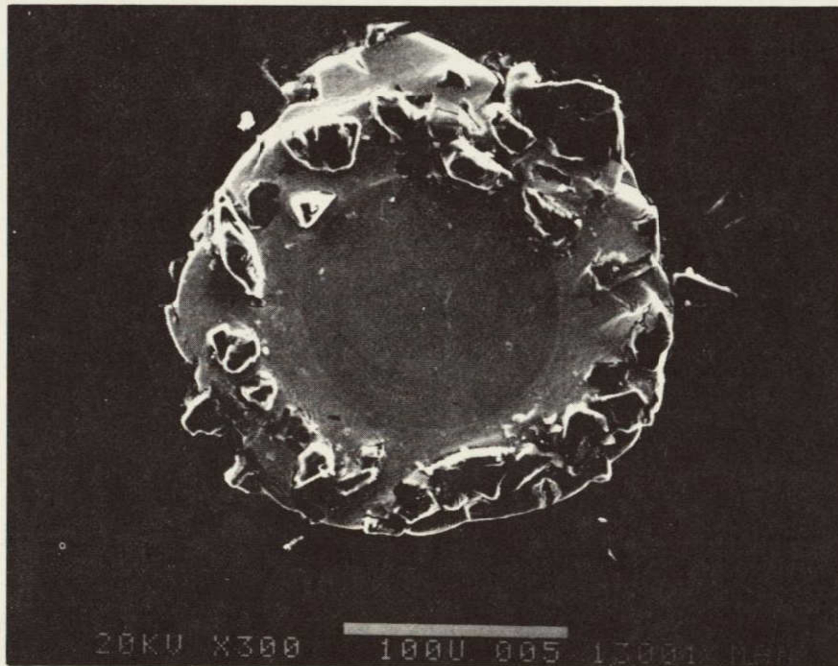

Figure 16. SEM View of Longitudinal Section and Cross-section of Diamond-plated Wire Showing Very High Diamond Concentration

hence their life was rather limited. It was found that nickel plating of these wires extended the life of the blades, however, a 0.5 mil, 12.5 μm thick plating was sufficient to bury the diamonds. Moreover the kerf obtained with commercially available impregnated wires was similar to the electroplated wires. Techniques were developed at Crystal Systems, Inc. to impregnate diamonds into copper sheaths on tungsten core wire. It was possible to impregnate 45 μm diamonds into 7.5 μm thick copper sheath. Further with this approach it was possible to impregnate diamonds only into the cutting edge. The use of these approaches has resulted in reducing the kerf to 6.2 mil, 0.155mm. The use of a thinner copper sheath will allow a thicker nickel plating, thereby preventing diamond pull-out and reduce kerf. It has also been found that the hardness of the nickel plating also affects the life of the blade.

(iii) Testing

The multi-wire FAST concept has been demonstrated on a machine designed for MBS slicing. With this machine the stroke length and rocking angle are limited so only small-sized workpieces could be cut. In addition the surface speed is limited to 100 ft/min due to the massive blade head. This is not optimum for diamond cutting.

In spite of the program being machine limited so far, significant advances have been made using this approach:

a) 64 wafers per inch, 25 wafers per cm

b) Conversion rates: 1.08 m^2/kg

CONCLUSIONS

1. Solar cells fabricated out of HEM cast silicon have shown conversion efficiencies of up to 15% (AM1). This has been achieved without optimization of material or cell processing parameters.

2. The silicon carbide impurities formed during melting of silicon in vacuum are associated with the use of graphite retainers. A reduction of 50% in carbon content was achieved by replacing graphite with molybdenum retainers.

3. The oxygen content of vacuum cast HEM silicon is lower than typical Czochralski grown silicon.

4. High solar cell efficiencies were obtained even with the use of unpurified graphite parts in the HEM furnace.

5. Turbulence obtained in the melt during growth cycle is associated with trapping of liquid silicon. This has been eliminated by altering the heat flow conditions.

6. A study to evaluate various graphites as heat transfer plugs has shown that ATJ graphite is best suited for the HEM environment.

7. Natural diamonds with sharp edges slice more efficiently than "blocky" synthetic diamonds.

8. Commercially impregnated wire has a thick copper sheath which prevents nickel plating to sufficient thickness to prevent diamond pull-out without burying the diamonds.

9. It is possible to impregnate 45 μm diamonds into the cutting edge only in a 7.5 μm thick copper sheath. However such a thin sheath is deformed during impregnation. Copper sheaths of 12.5 μm and 15 μm thickness do not show deformation.

10. Electroless nickel plating of wires impregnated in cutting edge only show nickel build-up around diamonds. This may help in achieving lower kerf.

11. Initial testing of the high speed slicer has shown that higher speeds and longer stroke are possible with vibration isolation. Slicing of large workpieces will be carried out shortly.

REFERENCES

1. F. Schmid and C. P. Khattak, "Heat Exchanger Method--Ingot Casting/Fixed Abrasive Method--Multi-Wire Slicing (II)," DOF'JPL 954373, Crystal Systems, Inc., Quarterly Progress F port No. 3, July 15, 1978.

2. F. Schmid and C. P. Khattak, "Heat Exchanger Method--Ingot Casting/Slicing Process, "ERDA/JPL 954373, Crystal Systems, Inc., Final Report (I), December 1, 1977.

3. F. Schmid and C. P. Khattak, "Heat Exchanger Method--Ingot Casting/Fixed Abrasive Method--Multi-Wire Slicing (II)," DOE/JPL 954373, Crystal Systems, Inc., Monthly Progress Report No. 5, August 15, 1978.

4. S. L. Zerfoss, R. Johnson and P. H. Egli, "Crystal Growth at High Temperatures," Trans. Faraday Soc., 1949.

5. D. I. Walker, Analytical Chemistry 22, 297 (1950).

6. F. Schmid, C. P. Khattak, T. G. Digges, Jr., and L. Kaufman, "Origin of SiC Impurities in Silicon Crystals Grown from the Melt in Vacuum," Journal of the Electro-Chemical Society (in press).

7. R. G. Newman and J. Wakefield, "Metallurgy of Semiconductor Materials," Interscience Publ., New York (1962).

8. H. W. Gutsche and D. E. Hill, "Determination of a Definition of Solar Grade Silicon," ERDA/JPL 954338, Monsanto Research Corporation, Final Report, September, 1976.

9. S. N. Rea and P. S. Gleim, "Large Area Czochralski Silicon," ERDA/JPL 954475, Texas Instruments, Inc., Final Report, April, 1977.

10. T. G. Digges, Jr., M. H. Leipold, K. M. Koliwad, G. Turner and G. D. Cumming, "Some Observations on the Characteristics of Low-cost Silicon Sheets," 5th IEEE Photovoltaic Specialists Conference, Baton Rouge, LA, 1976.

11. F. Schmid and C. P. Khattak, "Heat Exchanger-Ingot Casting/Slicing Process," ERDA/JPL 954373, Crystal Systems, Inc., Quarterly Technical Progress Report No. 8 (Phase I), October, 1977.

12. F. Schmid and C. P. Khattak, "Heat Exchanger Method--Ingot Casting/Fixed Abrasive Method--Multi-Wire Slicing (II)," DOE/JPL 954373, Crystal Systems, Inc., Quarterly Progress Report No. 2, April 7, 1978.

13. R. W. Aster and R. G. Chamberlain, "Interim Price Estimation Guidelines: A Precursor and an Adjunct to Samics III," LSSA Project, JPL Publ. 5101-33, September 10, 1977.

14. K. M. Koliwad, M. H. Leipold, G. D. Cumming, and T. G. Digges, Jr., "Economic Analysis of the Cost of Silicon Sheet Produced from Czochralski Grown Material," IEEE Photovoltaic Specialists Conference, Baton Rouge, LA (1976).

15. H. Yoo, R. Schwartz and P. Iles, "Analysis of ID Slicing of Silicon for Low-Cost Solar Cells," Proc. 13th IEEE Photovoltaic Specialists Conf., Washington, D.C. (1978).

MILESTONES

ITEM	DESCRIPTION	1977 N	D	1978 J	F	M	A	M	J	J	A	S	O	N	D
1	2.5 kg HEM crack-free ingot/square cross-section greater than 10 cm x 10 cm														
2	Design/fabricate wafering machine														
3	Ingot samples/wafer samples														
4	Characterization														
5	Crucible development														
6	Crucible cost studies														
7	Growth rate studies														
8	Blade development														
9	Fabricate/evaluate solar cells														
10	Design analysis study														
11	Monthly report														
12	Quarterly report														
13	Annual report														

ORIGINAL PAGE IS
OF POOR QUALITY